



HAL
open science

An efficient and robust staggered algorithm applied to the quasi-static description of brittle fracture by a phase-field approach

Ye Lu, Thomas Helfer, Benoît Bary, Olivier Fandeur

► **To cite this version:**

Ye Lu, Thomas Helfer, Benoît Bary, Olivier Fandeur. An efficient and robust staggered algorithm applied to the quasi-static description of brittle fracture by a phase-field approach. *Computer Methods in Applied Mechanics and Engineering*, 2020, 370, pp.113218. 10.1016/j.cma.2020.113218. hal-03105959

HAL Id: hal-03105959

<https://hal.science/hal-03105959v1>

Submitted on 18 Jul 2022

HAL is a multi-disciplinary open access archive for the deposit and dissemination of scientific research documents, whether they are published or not. The documents may come from teaching and research institutions in France or abroad, or from public or private research centers.

L'archive ouverte pluridisciplinaire **HAL**, est destinée au dépôt et à la diffusion de documents scientifiques de niveau recherche, publiés ou non, émanant des établissements d'enseignement et de recherche français ou étrangers, des laboratoires publics ou privés.



Distributed under a Creative Commons Attribution - NonCommercial 4.0 International License

An efficient and robust staggered algorithm applied to the quasi-static description of brittle fracture by a phase-field approach

Ye Lu^{a,*}, Thomas Helfer^a, Benoît Bary^b, Olivier Fandeur^c

^aCEA, DEN, DEC, SESC, LSC, Cadarache, France

^bCEA, DEN, DPC, SECR, LECBA, Saclay, France

^cCEA, DEN, DM2S, SEMT, LM2S, Saclay, France

Abstract

The phase field method has been widely adopted in brittle fracture analysis for its ability to handle complex crack topology. This paper presents a novel efficient and robust phase field algorithm for quasi-static brittle fracture analysis. This algorithm overcomes two major issues that affect significantly the numerical cost of the method: the treatment of **unstable discontinuous** crack propagation and the inequality constraint associated with the irreversibility of the damage evolution. To handle **unstable discontinuous** crack propagation, a semi-implicit scheme, which combines the usual explicit and implicit schemes, is proposed. Different from explicit schemes that require small time steps and purely implicit schemes that **lose** immediately efficiency when encountering **unstable crack discontinuous** propagation, the proposed method can **release alleviate** the steps constraint while keeping a good robustness with discontinuous cracking. Concerning the irreversibility constraint, this work proposes a practical and easy-to-implement method. It is shown that this method is extremely efficient and robust without any supplementary numerical coefficient. The efficiency of the method is demonstrated by means of representative numerical examples.

Keywords: Phase field, Brittle fracture, **Discontinuous crack** propagation, Semi-implicit algorithm, Irreversibility implementation

*Corresponding author

Email addresses: ye.lu@cea.fr (Ye Lu), thomas.helfer@cea.fr (Thomas Helfer), benoit.bary@cea.fr (Benoît Bary), olivier.fandeur@cea.fr (Olivier Fandeur)

Preprint submitted to Computer Methods in Applied Mechanics and Engineering March 1, 2020

1 **1. Introduction**

2 Numerical simulations of fracture processes play an important role in
3 engineering designs. The prediction of crack propagation in brittle materials
4 is usually based on Griffith's theory [1], which compares the energy released
5 by the crack propagation to a critical energy release rate. A general concept
6 in these models is that a necessary condition for crack propagation is that the
7 energy release rate reaches a critical value. Discontinuous crack propagation
8 happens when the elastic energy stored in the body is greater than this value.

9 One of the major difficulties in fracture simulations is the intrinsic spa-
10 tial singularity, i.e. ~~the displacement field is discontinuous across the~~
11 ~~crack point~~ ~~the crack tip~~. The numerical treatment of this singularity in
12 finite element (FE) models can be considered, either by embedding disconti-
13 nuity lines by means of remeshing strategies [2, 3] and cohesive elements [4, 5],
14 or by enriching the displacement field with discontinuities using the parti-
15 tion of unity method [6], as introduced in extended finite element methods
16 (XFEM) [7]. However, tracing the evolution of complex crack paths, includ-
17 ing crack initiation, propagation, merging and branching, in such models has
18 proven to be a tedious task, especially in three dimensional cases [8, 9].

19 An alternative approach to deal with the discontinuous crack topology
20 consists in incorporating a smooth auxiliary (phase) field. This auxiliary
21 variable describes continuously the transition between fully broken and intact
22 material phases within a small band. As a consequence, discontinuities are
23 not directly introduced into the model, the evolution of fracture surfaces
24 is provided by the problem solution on a fixed mesh. This is particularly
25 advantageous for handling complex crack paths. Following the terminology
26 of [10], such regularized models are referred to as phase field models.

27 Phase field models of quasi-static brittle fracture are based on the vari-
28 ational formulation of Griffith's-type methods, proposed by Francfort and
29 Marigo [11] and implemented for the first time by Bourdin et al. [12]. The
30 energy functional in the phase field model resembles closely the potential
31 used in image segmentation [13], which relies on the regularization concept
32 through Γ -convergence [14]. More recently, Miehe et al. [10, 15] presented a
33 quasi-static phase field formulation aligned with thermodynamic arguments.
34 This model possesses several practical features for its numerical implementa-
35 tion and has been widely adopted for various applications (see e.g. [16, 17]).

36 A higher-order extension within the isogeometric analysis framework can be
37 found in [18].

38 The major limit of the phase field method for engineering-size applica-
39 tions is its expensive computational cost. Phase field models usually require
40 very fine meshes around crack paths for convergence reasons. Although par-
41 allelization [19] or adaptive meshing strategies [20, 21, 22, 23, 24, 25] can
42 be applied to accelerate the simulations, the development of efficient solu-
43 tion schemes remains a key point to make the method more attractive for
44 problems having real engineering interests.

45 Depending on whether the displacement and the crack field are computed
46 simultaneously or **alternativelyalternately**, two families of phase field solu-
47 tion schemes can be distinguished: monolithic and staggered schemes. Mono-
48 lithic schemes are expected to have higher convergence rates, since the two
49 field solutions are solved simultaneously in a unique Newton-Raphson loop.
50 However, this type of approaches suffers from the well-known **discontinu-**
51 **ous** crack propagation in quasi-static simulations. The loss of convexity of
52 the problem makes the solutions difficult to converge. Additional numerical
53 treatments are usually required to improve its robustness (see e.g. [26]). Fur-
54 thermore, this approach cannot be directly implemented into a commercial
55 code without supplementary developments.

56 Staggered schemes are more robust and easier to implement in an ex-
57 isting commercial code [27]. They are based on an operator split algo-
58 rithm in which the mechanical problem and the damage problem are solved
59 **alternativelyalternately**. Explicit or implicit strategies can then both be
60 considered. Explicit schemes [10, 16] consider that the damage is constant
61 over an incremental time step when computing the displacement field. The
62 damage field is updated for the next time step after the convergence of the
63 mechanical problem. They were found to be extremely robust, even with
64 **discontinuous** crack propagation. Nevertheless, this kind of approaches
65 usually requires very small time steps, which are not accessible for many
66 engineering applications.

67 Implicit schemes can **overcomealleviate** this time step dependency (see
68 e.g. [28, 29, 30]). The implicit method proposed by [28, 29] is usually known
69 as an alternate minimization scheme, in which two minimization problems for
70 the displacement and damage fields are solved independently by fixing one of
71 these two fields. Similarly to explicit schemes, this method computes the dis-
72 placement field at constant damage, but instead updates the latter at current
73 time step and then computes again a new displacement. Therefore, different

74 from the explicit scheme, the convergence of damage field can be ensured
75 for each time step in the alternate minimization procedure. This method
76 is very stable but usually converges extremely slowly, although relaxation
77 methods can be employed to accelerate it [31]. Experience [30] shows that
78 the implicit methods work ~~independently of~~with relatively large time
79 steps but usually require numerous iterations to find the converged solutions,
80 particularly when encountering ~~unstable~~discontinuous crack propagation.
81 Nevertheless, this kind of approaches is appealing for many engineering prob-
82 lems subjected to long-term loading (e.g. nuclear fuel simulations [30]), in
83 which small time steps are not acceptable.

84 This work falls within this perspective. In order to have a solution scheme
85 ~~independent of~~allowing large time steps while keeping a good efficiency
86 and robustness for ~~unstable propagation~~discontinuous cracking, we
87 present here a novel staggered scheme, referred to as semi-implicit method,
88 for quasi-static brittle fracture simulations. The first important ingredient
89 of the semi-implicit method relies on ~~an alternative~~a modified one-loop
90 implicit scheme [30], in which we suggest to integrate the damage update into
91 the mechanical Newton loop so as to improve the damage convergence rate.
92 Since the damage field is updated after computing each displacement incre-
93 ment ~~estimate~~, the convergence of the mechanical problem may be strongly
94 perturbed but we can expect a faster damage convergence, compared to the
95 alternate minimization scheme [28, 29]. Indeed, as shown in the examples,
96 damage field can converge relatively faster than displacement field, and even
97 small variations of the damage field can affect significantly the mechani-
98 cal equilibrium. Particularly in ~~unstable~~discontinuous propagation steps,
99 globally stable damage field cannot ensure immediately ~~that~~ equilibrium.
100 We observed that this problem causes a significant number of iterations only
101 needed for achieving that mechanical convergence, after the convergence of
102 damage field. A simple way for overcoming this problem is to switch to a less
103 strict convergence criterion for the mechanical problem. However, this is not
104 considered in this work. Instead, on the level of solution scheme, this work
105 proposes to apply an explicit-type resolution for the mechanical convergence
106 by fixing the damage variables, once the damage convergence is found by the
107 suggested implicit procedure. Therefore, this semi-implicit scheme, which
108 combines the implicit and explicit schemes, presents a twofold advantage:
109 large time steps ~~independence~~ and robustness for discontinuous cracking.

110 Another important issue in phase field implementation to deal with is the
111 irreversibility condition. The thermodynamics arguments demand that the

112 crack field should not be reversible in any case. This results in an inequality-
113 constrained phase field problem. Different methods to impose the irreversibil-
114 ity can significantly affect the computational cost of phase field solutions.
115 The simplest way, proposed by Miehe et al. [10], is to introduce a mono-
116 tonically increasing history field energy function in the phase field equation
117 to replace the original loading-induced reference energy. This method seems
118 very efficient, since no explicit constraints are introduced in the phase field
119 equation. However, the introduction of the history field makes the phase field
120 solution differ from the original variational framework and its equivalence to
121 the original minimization problem can not be proven [32]. From this view-
122 point, the penalty methods [32], which rely on equality-based formulations
123 and can keep the variational nature of the original problem, seem an appeal-
124 ing option. The main drawback of these methods lies on the introduction
125 of the penalty coefficient, which may cause ill-conditioning of the problem.
126 Although analytic derivations of the 'optimal' coefficients have been pro-
127 posed, the choice of these penalty coefficients remains a delicate task. The
128 most standard method to solve the constrained phase field problem is the La-
129 grangian method or its augmented version [33]. This kind of methods may
130 result in a large size system and therefore an extremely high numerical cost,
131 with the introduction of a large amount of extra-variables. Hence, this kind
132 of methods needs an efficient implementation.

133 This work proposes an efficient way to impose the irreversibility condition,
134 which can be viewed as an efficient variant of Lagrangian method for the
135 inequality-constrained phase field problem. Hence, this method can keep the
136 original variational nature of the phase field solution. The implementation
137 relies on an iterative procedure with only equality constraints on a reduced
138 and irreversible active subset, which limits the size of the augmented system.
139 Particularly, a vanishing energy driving force is applied to the constrained
140 subset, which ensures the positivity of Lagrange multipliers. It is shown that
141 the proposed method is very efficient and can lead to a similar result to that
142 of Lagrangian method. Together with the proposed semi-implicit solution
143 scheme, the novel phase field algorithmic implementation seems very robust
144 for quasi-static brittle fracture simulations. Several representative numerical
145 examples will be presented for demonstrating the efficiency and robustness
146 of the method.

147 This paper is organized as follows. Section 2 introduces the phase field
148 formulation for brittle fracture, in which the novel method for imposing the
149 irreversibility condition is described. Then, the semi-implicit solution scheme

150 is exposed in Section 3. Section 4 will present some numerical examples.
 151 Finally, the paper will be closed by some concluding remarks.

152 2. Problem formulation

153 2.1. Phase field modeling of crack topology

154 Let us consider a n dimensional domain $\Omega \subset \mathbb{R}^n$ with a fully open crack
 155 $\Gamma \subset \mathbb{R}^{n-1}$. The crack field can be then described by a damage function $d(x)$
 156 which is equal to 0 everywhere, except for Γ . For a fully damaged point, we
 157 consider that d equals to 1. Figure 1(a) shows a sharp crack topology. Dif-
 158 fuse approximation consists in introducing a continuous transition between
 159 the crack and undamaged zone. This leads to a partially damaged domain
 160 around the crack, in which $d \in (0, 1)$ (see e.g. Figure 1(b)). In phase field
 161 methods [12, 10], the width of the damaged zone is controlled by an inter-
 162 nal characteristic length l_c (called also regularization length) and the crack
 163 surface density can be defined as

$$\gamma(d, \nabla d) = \frac{1}{2l_c}(d^2 + l_c^2|\nabla d|^2) \quad (1)$$

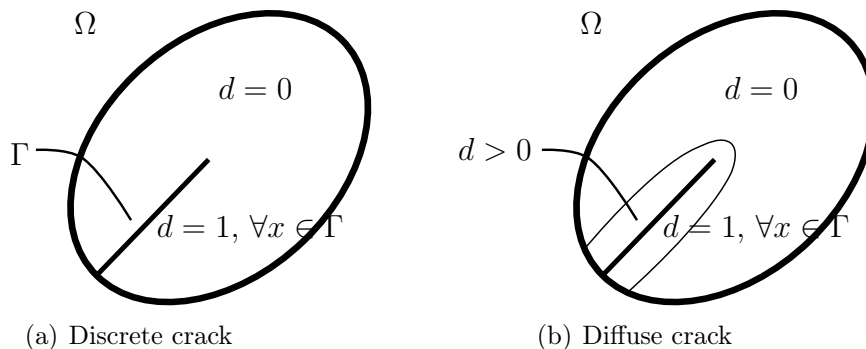


Figure 1: Approximation of crack topology

164 As a consequence, the total crack surface is approximated by its integral
 165 over the domain

$$\Gamma \approx \Gamma(d) = \int_{\Omega} \gamma(d, \nabla d) dV = \int_{\Omega} \frac{1}{2l_c}(d^2 + l_c^2|\nabla d|^2) dV \quad (2)$$

166 *2.2. Variational formulation and governing equations*

167 The variational formulation of brittle fracture is given by the work of
 168 Francfort and Marigo [11]. Let Ω denote again the elastic body with a crack
 169 Γ , a prescribed surface loading $\bar{\mathbf{t}}$ is applied on its boundary $\partial\Omega$, the energy
 170 functional in quasi-static setting reads

$$\Pi(\mathbf{u}, \Gamma) = \underbrace{\int_{\Omega} \psi_e(\boldsymbol{\varepsilon}_e(\mathbf{u}))dV}_{\Pi_e} + \underbrace{\int_{\Gamma} G_c d\Gamma}_{\Pi_d} - \underbrace{\int_{\partial\Omega} \bar{\mathbf{t}}\mathbf{u}dA}_{\Pi_{\text{ext}}} \quad (3)$$

171 where \mathbf{u} denotes the displacement field, G_c is the critical release energy per
 172 unit crack surface, and Π_e , Π_d , Π_{ext} denote respectively the elastic bulk en-
 173 ergy, dissipation potential and external work. **In this work, no external**
 174 **applied forces are taken into account. Hence, we can simply con-**
 175 **sider $\bar{\mathbf{t}} = 0$ without changing the formulation.** According to Griffith's
 176 theory, cracks should propagate along a path of the least energy and satisfy
 177 the irreversibility condition: $\Gamma(s) \subseteq \Gamma(t)$, $\forall s < t$, which leads to a minimiza-
 178 tion problem for crack propagation

$$(\mathbf{u}, \Gamma) = \text{Arg} \left\{ \inf_{\mathbf{u}^*, \Gamma^*} \Pi(\mathbf{u}^*, \Gamma^*) \right\} \quad (4)$$

179 We remark that the volume body forces are neglected here. Under in-
 180 finitesimal strain assumption, the elastic strain tensor is defined as

$$\boldsymbol{\varepsilon}_e = \boldsymbol{\varepsilon} = \nabla_s \mathbf{u} \quad (5)$$

181 where ∇_s denotes the symmetric gradient operator.

182 The dissipation functional is defined as the work needed to create the
 183 corresponding crack surface Γ which is approximated by $\Gamma(d)$ in diffuse ap-
 184 proximation, i.e.

$$\Pi_d = \int_{\Gamma} G_c d\Gamma \approx \int_{\Gamma} G_c \gamma(d, \nabla d) d\Gamma \quad (6)$$

185 In order to be consistent with the second thermodynamic principle, we
 186 demand a positive crack dissipation rate: $\dot{\Pi}_d \geq 0$. This results in

$$\delta_d \gamma \geq 0 \quad \text{and} \quad \dot{d} \geq 0 \quad (7)$$

187 where $\delta_d \gamma = \frac{1}{l_c} (d - l_c^2 \Delta d)$. Note that this positive increment constraint
 188 (7) ensures the global irreversibility condition of Γ . In addition, the first
 189 condition in (7) is automatically satisfied in phase field approximation.

190 Taking into account the rigidity degradation of material due to the frac-
 191 ture and a spectral decomposition of strain tensor [10] for preventing the
 192 crack opening in compression, we can define the elastic energy functional as

$$\Pi_e = \int_{\Omega} (g(d)\psi_e^+(\boldsymbol{\varepsilon}) + \psi_e^-(\boldsymbol{\varepsilon})) dV \quad (8)$$

193 where the degradation function is chosen as: $g(d) = (1-d)^2 + k$, with a small
 194 value k appearing to avoid singular problems. **In our work, this value is**
 195 **set to 10^{-10} .** The spectral decomposition of strain is written as

$$\boldsymbol{\varepsilon} = \boldsymbol{\varepsilon}^+ + \boldsymbol{\varepsilon}^- \quad \text{with } \boldsymbol{\varepsilon}^{\pm} = \sum_{i=1} \langle \varepsilon_i \rangle^{\pm} \mathbf{n}_i \otimes \mathbf{n}_i \quad (9)$$

196 where $(\cdot)^+$ and $(\cdot)^-$ denote respectively the tensile and compressive modes.
 197 ε_i and \mathbf{n}_i are the eigenvalues and eigenvectors in different dimensions. The
 198 Macaulay brackets are defined as: $\langle \cdot \rangle^{\pm} = \frac{1}{2}(\cdot \pm |\cdot|)$. With the Lamé constants
 199 λ and μ , the elastic energy relating to each part of strain is defined as

$$\psi_e^{\pm}(\boldsymbol{\varepsilon}) = \frac{\lambda}{2} (\langle \text{tr}[\boldsymbol{\varepsilon}] \rangle^{\pm})^2 + \mu \boldsymbol{\varepsilon}^{\pm} : \boldsymbol{\varepsilon}^{\pm} \quad (10)$$

200 Therefore, considering that $\Pi_e = \int_{\Omega} \Psi_e dV = \int_{\Omega} (\boldsymbol{\sigma} : \boldsymbol{\varepsilon} - fd) dV$, the
 201 definition of stress is given by

$$\boldsymbol{\sigma} = \frac{\partial \Psi_e}{\partial \boldsymbol{\varepsilon}} = g(d) (\lambda \langle \text{tr}[\boldsymbol{\varepsilon}] \rangle^+ \mathbf{I} + 2\mu \boldsymbol{\varepsilon}^+) + \lambda \langle \text{tr}[\boldsymbol{\varepsilon}] \rangle^- \mathbf{I} + 2\mu \boldsymbol{\varepsilon}^- \quad (11)$$

202 and the energetic driving force of damage reads

$$f = -\frac{\partial \Psi_e}{\partial d} = 2(1-d)\psi_e^+ \quad (12)$$

203 Taking the variation of the total energy functional, the optimization prob-
 204 lem (4) with inequality constraint becomes [10]:

$$\begin{cases} \text{div } \boldsymbol{\sigma} = 0 & \text{in } \Omega \\ \boldsymbol{\sigma} \cdot \mathbf{n} = \bar{\mathbf{t}} & \text{on } \partial_{\sigma} \Omega \end{cases} \quad (13)$$

205 with a Kuhn-Tucker-type (KT) condition

$$\dot{d} \geq 0, \quad f - G_c \delta_d \gamma \leq 0, \quad \dot{d}(f - G_c \delta_d \gamma) = 0 \quad (14)$$

206 in the whole domain Ω and $\nabla d \cdot \mathbf{n} = 0$ on the boundary $\partial\Omega$. Note that the
 207 equation (14)₃ allows to compute the damage d when $\dot{d} > 0$, i.e.

$$f - G_c \delta_d \gamma = 0 \quad \rightarrow \quad 2(1-d)\psi_e^+ = \frac{G_c}{l_c} (d - l_c^2 \Delta d) \quad \text{for } \dot{d} > 0 \quad (15)$$

208 *2.3. Finite element discretization*

209 The implementation of phase field method can be performed in different
 210 manners (monolithic or staggered), as mentioned in introduction. For the
 211 reason of stability and robustness, this work is based on a operator split
 212 scheme, i.e. staggered implementation [10].

213 The finite element method is used for the spatial discretization.

$$\mathbf{u}(x) = \mathbf{N}_u(x)\mathbf{U}, \quad d(x) = \mathbf{N}_d(x)\mathbf{d} \quad (16)$$

214 where \mathbf{U} and \mathbf{d} are respectively the usual nodal displacement and damage
 215 vectors. \mathbf{N}_u and \mathbf{N}_d are corresponding FE shape functions. Noting by \mathbf{B} the
 216 gradient of shape functions, the FE discretization leads to the two following
 217 equations (17) et (18):

$$\mathbf{R}^u(\mathbf{u}, d, t) = \frac{\partial \Pi}{\partial \mathbf{u}} = \frac{\partial \Pi_e}{\partial \mathbf{u}} - \frac{\partial \Pi_{\text{ext}}}{\partial \mathbf{u}} = \mathbf{F}_{\text{int}}(\mathbf{u}, d) - \mathbf{F}_{\text{ext}}(t) \quad (17)$$

218 where $\mathbf{F}_{\text{int}} = \int_{\Omega} \mathbf{B}_u^T \boldsymbol{\sigma} dV$, $\mathbf{F}_{\text{ext}} = \int_{\partial\Omega} \mathbf{N}_u^T \bar{\mathbf{t}} dA$.

$$\mathbf{R}^d(\mathbf{u}, d) = \frac{\partial \Pi}{\partial d} = \frac{\partial \Pi_e}{\partial d} + \frac{\partial \Pi_d}{\partial d} = \mathbf{K}_d(\mathbf{u})\mathbf{d} - \mathbf{F}_d(\mathbf{u}) \quad (18)$$

219 where $\mathbf{K}_d = \int_{\Omega} (2\psi_e^+ + \frac{G_c}{l_c}) \mathbf{N}_d^T \mathbf{N}_d dV + \int_{\Omega} G_c l_c \mathbf{B}_d^T \mathbf{B}_d dV$, $\mathbf{F}_d = \int_{\Omega} 2\mathbf{N}_d^T \psi_e^+ dV$.

220 The solution (\mathbf{u}, d) to the original variational problem (4) should
 221 be computed through minimizing the residuals \mathbf{R}^u and \mathbf{R}^d under
 222 the irreversibility condition $\dot{d} \geq 0$. Due to the splitting of the
 223 energy (11), the mechanical problem (17) remains nonlinear even
 224 when fixing the damage variable at a constant stage. The stan-
 225 dard Newton–Raphson method is usually applied for the mechan-
 226 ical problem.

227 *2.4. Irreversibility condition*

228 As the reference elastic energy ψ_e^+ can decrease with external loading, the
 229 desired condition: $\dot{d} \geq 0$ in Ω is not automatically satisfied in the method.
 230 Hence, this point needs some additional treatment. To this end, different
 231 methods exist in the literature.

232 *2.4.1. Brief review of previous methods*

233 The most thorough way from the mathematical point of view is to apply
 234 an inequality constraint when solving the phase field equation

$$2(1-d)\psi_e^+ = \frac{G_c}{l_c} (d - l_c^2 \Delta d) \quad \text{subject to} \quad \dot{d} \geq 0 \quad (19)$$

235 As mentioned in the introduction, this inequality constraint can be enforced
 236 using the Lagrange multiplier (see e.g. [28, 33]). However, the standard
 237 Lagrangian method results in a large size augmented system, which is ex-
 238 tremely expensive to solve. Its application to an engineering size problem is
 239 inappropriate. An alternative option is to use the penalty method [32] which
 240 does not introduce extra-variables in the problem. However, the introduction
 241 of penalty coefficients may result in ill-conditioned systems.

242 A more efficient way [12] is to solve the phase field equation (18) with
 243 a constraint on the damage variation only when a point reaches a critical
 244 value, i.e.

$$\dot{d} = 0 \quad \text{for} \quad d \approx 1 \quad (20)$$

245 Therefore, this method only prevents the cure of fully broken points. The
 246 irreversibility condition is not ensured in the whole domain Ω .

247 An alternative efficient method [34] consists in solving, at first, only the
 248 unconstrained phase field equation (18) for the whole domain Ω , and then
 249 doing an a posteriori projection, which reads

$$\begin{cases} 2(1-d^*)\psi_e^+ = \frac{G_c}{l_c} (d^* - l_c^2 \Delta d^*) \\ d(t) = \max(d^*, d(s)), \quad \forall s < t \end{cases} \quad (21)$$

250 This method enforces the exact irreversibility condition, but the projection
 251 makes the solution deviate from the original variational framework.

252 More recently, Miehe et al. [10] proposed to introduce a compact history
 253 field function \mathcal{H} to replace the reference elastic energy ψ_e^+ in phase field
 254 equation, which results in

$$\begin{cases} \mathcal{H} = \max(\psi_e^+(t), \psi_e^+(s)), \quad \forall s < t \\ 2(1-d)\mathcal{H} = \frac{G_c}{l_c} (d - l_c^2 \Delta d) \end{cases} \quad (22)$$

255 In this method, the increasing of damage is driven by the history field function
 256 \mathcal{H} . The following KT condition is expected to be satisfied in Ω

$$\dot{d} \geq 0, \quad \psi_e^+ - \mathcal{H} \leq 0, \quad \dot{d}(\psi_e^+ - \mathcal{H}) = 0 \quad (23)$$

257 As commented by [10], the damage will not decrease with the monotonically
 258 increasing function \mathcal{H} , therefore the irreversibility $\dot{d} \geq 0$ can be always en-
 259 sured. However, nothing can guarantee the consistency condition (23)₃: the
 260 equation (22) does not guarantee that the damage will not increase with a
 261 decreasing reference energy ψ_e^+ . Indeed, the introduction of the history field
 262 function, which can be viewed as an a priori projection, makes the solution
 263 lose its original variational nature. Regardless of this drawback, this method
 264 has been widely adopted for its implementation simplicity and efficiency.

265 *2.4.2. An efficient irreversibility implementation*

266 In order to keep at maximum the variational nature of the phase field
 267 solutions without losing much efficiency, we propose here a novel implemen-
 268 tation of the inequality condition. Let us consider a time discrete formulation
 269 of the constrained damage problem (19), the damage at instant t is given by

$$2(1 - d_t)\psi_e^+ = \frac{G_c}{l_c} (d_t - l_c^2 \Delta d_t) \quad \text{subject to} \quad d_t \geq d_{t-1} \quad (24)$$

270 The use of standard Lagrangian method leads to the following equations
 271 with equality constraints on a set of points

$$\begin{cases} 2(1 - d_t)\psi_e^+ + \gamma = \frac{G_c}{l_c} (d_t - l_c^2 \Delta d_t) \\ \gamma(d_t - d_{t-1}) = 0 \\ \gamma \geq 0 \end{cases} \quad (25)$$

272 where γ denotes the Lagrange multiplier, which should not be negative:
 273 $\gamma \geq 0$. The solution of the above equations can be found by an iterative
 274 procedure, in which the values of Lagrange multipliers are updated accord-
 275 ing to the current estimate and successively until all the constrained points
 276 have positive damage increments. This procedure is extremely expensive for
 277 two reasons: introduction of a large number of additional variables (which
 278 is equal to the degree number of original system) and numerous iterations
 279 required for finding the a priori unknown values of Lagrange multipliers. **Al-**
 280 **though active-set algorithms (e.g. [22]) can be used to reduce the**
 281 **additional variables, the iterations number may remain important.**

282 In this work, we propose an efficient solution procedure with only equality
 283 constrains on a subset of the global system, which is based on the following

284 modified formulation

$$\begin{cases} 2(1 - d_t)(1 - p)\psi_e^+ + p\gamma = \frac{G_c}{l_c} (d_t - l_c^2 \Delta d_t) \\ \gamma(d_t - d_{t-1}) = 0 \\ \gamma \geq 0 \\ \gamma(1 - p) = 0 \end{cases} \quad (26)$$

285 where p is an indicator function which equals to 1 for the constrained subset
 286 and equals to 0 for the unconstrained subset. The first equation implies
 287 that the energetic driving force $f = \frac{\partial \Psi_e}{\partial d}$ (12) should be vanishing for the
 288 constrained points. This supplementary condition: $f = 0$ ($\psi_e^+ = 0$) has
 289 a minor effect on those unconstrained points. Hence, the final phase field
 290 solution is expected to keep the original variational nature. This formulation
 291 enables the following solution procedure:

- 292 • Given a precomputed energy ψ_e^+ and the previous damage d_{t-1}
- 293 • Initiation: $p(x) = 0, \forall x \in \Omega$
- 294 • For iteration i
 - 295 1. Compute the damage d_i^* with $d_i^* = d_{t-1}$ on the constrained set
 296 $\mathcal{D} = \{x \in \Omega \mid p(x) = 1\}$
 - 297 2. Determine the decreasing points $\mathcal{D}^* = \{x \in \Omega \mid d_i^* < d_{t-1}\}$
 - 298 3. Update the constrained set $\mathcal{D} = \mathcal{D} \cup \mathcal{D}^*$
 - 299 4. Update the indicator function $p(x) = 1, \forall x \in \mathcal{D}$
 - 300 5. Check the convergence: If $\mathcal{D}^* = \emptyset$ or $\|d_i^* - d_{i-1}^*\|_\infty \leq \epsilon_c$, then
 301 $d_t = d_i^*$, END. Otherwise, repeat the iteration.

302 This procedure is computationally efficient, since only equality constraints
 303 are imposed on a subset of the global system. In addition, it should be
 304 noticed that the constrained set is irreversibly updated in the sense that
 305 one already constrained point cannot become unconstrained in a solution
 306 loop. The feasibility of this concept is ensured by the vanishing energetic
 307 driving force, which guarantees the positivity of the Lagrange multiplier.
 308 This way, the iterative procedure usually converges very fast within several
 309 iterations. The irreversibility condition: $\dot{d} \geq 0$ is automatically satisfied with
 310 the converged solution. Compared to those projection-based approaches (e.g.

311 [10, 34]), this method is more expensive but is expected to lead to more robust
312 variationally-consistent phase field solutions.

313 **The proposed implementation differs from active-set algorithms**
314 **in the following aspects. The constrained set is increasingly up-**
315 **dated for a given energy state: $\mathcal{D}^i \subset \mathcal{D}^{i+1}$, where i stands for the it-**
316 **eration step. However, in active-set algorithms, active constrained**
317 **points may be removed from the constrained set (e.g. according**
318 **to the positivity of the Lagrange multiplier), hence $\mathcal{D}^i \not\subset \mathcal{D}^{i+1}$. In**
319 **addition, the energy is removed for the constrained set in proposed**
320 **algorithm, which is not the case for active-set algorithms. The im-**
321 **port of this irreversibility implementation is numerically analyzed**
322 **by a 1D example in Appendix.**

323 **3. A robust solution scheme for unstable crack propagation**

324 *3.1. ~~Unstable~~Discontinuous crack growth*

325 In quasi-static crack modeling, ~~unstable crack propagation is present~~
326 ~~as a discontinuous crack evolution in time~~ discontinuous crack evo-
327 lution happens as the jump of the crack field. It remains a compu-
328 tationally challenging problem with standard iterative Newton algorithms,
329 since the jump of the solution (~~e.g. displacement field~~) is difficult to
330 capture with the tangent operator ~~due to the loss of convexity of the~~
331 ~~problem~~. One possible way to overcome this issue is to switch to truly dy-
332 namic simulations [35, 36, 37], in order to capture the loss of kinetic energy
333 which is not taken into account in quasi-static simulations. However, the nu-
334 merical integration scheme requires very small time steps for capturing the
335 stress waves. Although this issue can be overcome using for example mass
336 scaling techniques [38], this kind of dynamic approaches is not considered in
337 this work. Hence, the development of efficient solution schemes is essential
338 to deal with the **unstable discontinuous** crack propagation in quasi-static
339 simulations.

340 *3.2. Explicit scheme*

341 An efficient phase field solution scheme has been proposed by [10] and
342 improved by [16]. This kind of approaches, referred to as explicit scheme,
343 consists in solving the mechanical equation at a constant damage for each
344 time step. Once the converged mechanical solution obtained, the damage

345 is then updated for the next step. Since the mechanical and damage prob-
 346 lems are decoupled, the problem to be solved becomes convex. This method
 347 shows an excellent convergence property even when **unstable discontinu-**
 348 **ous** cracking occurs. However, as the convergence on damage is not checked,
 349 small time steps are usually demanded. The solution procedure is summa-
 350 rized as follows:

- 351 • At time step t , $d^* = d_{t-1}$
- 352 • Loop for mechanical equilibrium: **find \mathbf{u} by minimizing $\mathbf{R}^u(\mathbf{u}, d^*, t)$**
- 353 • If convergence, **update $\mathbf{u}_t = \mathbf{u}$ and internal variables**
- 354 • **Loop for** the damage problem: **find d by minimizing $\mathbf{R}^d(\mathbf{u}_t, d)$ with**
 355 **$\dot{d} \geq 0$**
- 356 • Update the damage field: $d_t = d$
- 357 • Pass to next time step

358 **We remark here the irreversibility condition is assumed to be con-**
 359 **sidered by one of the previously mentioned methods in section 2.4.**
 360 **This remark holds for the following sections.**

361 3.3. Implicit scheme

362 3.3.1. Alternate minimization scheme

363 In order to release the time step constraint, the convergence on damage
 364 field must be additionally checked. The alternate minimization scheme [28,
 365 29] is similar to the explicit scheme, but has an additional loop on the damage
 366 field before passing to the next step:

- 367 • At time step t , $d^0 = d_{t-1}$
- 368 • Loop on $j = 0, 1, 2, \dots$
 - 369 1. Loop for mechanical equilibrium: **find \mathbf{u} by minimizing $\mathbf{R}^u(\mathbf{u}, d^j, t)$**
 - 370 2. If convergence, **update $\mathbf{u}_t = \mathbf{u}$ and internal variables**
 - 371 3. **Loop for** the damage problem: **find d by minimizing $\mathbf{R}^d(\mathbf{u}_t, d)$**
 372 **with $\dot{d} \geq 0$**
 - 373 4. Update the damage field: $d^{j+1} = d$

- 374 5. If $\|d^{j+1} - d^j\| \leq \epsilon_d$, **then** $d_t = d^{j+1}$, pass to next time step
 375 6. **Otherwise, repeat the j -loop**

376 Some variants with different convergence criterion for damage field can also
 377 be found in the literature (e.g. [29, 32]). This scheme is stable **in the sense**
 378 **that the mechanical loop always converges within limited itera-**
 379 **tions**, thanks to the decoupling of the two problems. The main drawback is
 380 the low convergence rate **of the global damage field**.

381 *3.3.2. A modified one-loop implicit scheme*

382 Alternatively, we can consider an implicit method by integrating the dam-
 383 age update in the mechanical loop:

- 384 • At time step t , $\mathbf{u}^0 = \mathbf{u}_{t-1}$, $d^0 = d_{t-1}$
 385 • **Mechanical Newton loop** on $i = 0, 1, 2, \dots$
- 386 1. **Compute a displacement increment** $\delta \mathbf{u}^{i+1} = -\mathbf{K}_u^{-1} \mathbf{R}^u(\mathbf{u}_{t-1}, d^i, t)$
 - 387 2. **Update** $\mathbf{u}^{i+1} = \mathbf{u}_{t-1} + \delta \mathbf{u}^{i+1}$ **and internal variables**
 - 388 3. **Loop for the damage problem: find d by minimizing** $\mathbf{R}^d(\mathbf{u}^{i+1}, d)$
 389 **with $d \geq 0$**
 - 390 4. Update the damage field: $d^{i+1} = d$
 - 391 5. If convergence, **then** $\mathbf{u}_t = \mathbf{u}^{i+1}$, $d_t = d^{i+1}$, pass to next time step
 - 392 6. **Otherwise, repeat the Newton loop**

393 **where \mathbf{K}_u stands for the tangent stiffness matrix or the initial elastic**
 394 **stiffness matrix for the modified Newton method.**

395 Generally **speaking**, the iterative Newton procedure should be repeated
 396 until the convergence of both mechanical and damage problems. **In this**
 397 **one-loop scheme, a necessary condition for the global mechanical**
 398 **equilibrium is the convergence of the damage field. Therefore, the**
 399 **residual \mathbf{R}^u can be used as a global convergence criterion.** This algo-
 400 rithm is particularly attractive, since the integration of damage update **into**
 401 **the mechanical loop makes the two problems coupled in a stronger**
 402 **manner and should** be helpful for **the global** convergence. In addition,
 403 the acceleration techniques [39] available for the mechanical convergence can
 404 be easily applied to accelerate the global convergence.

405 This approach has been implemented for a phase field modeling of nuclear
 406 fuel [30]. For overcoming the **discontinuous** propagation steps, a fictive

407 path loading method [40] is employed in that implementation. This method
 408 consists in accepting unstable states during the propagation and re-starting
 409 the iteration by considering the displacement increment $\delta \mathbf{u}^0$ equals to zero.
 410 It is shown that this implicit scheme can find a solution **of the non-convex**
 411 **problem** with an important number of iterations for the **discontinuous**
 412 crack propagation. Furthermore, we observed that many iterations are per-
 413 formed after the convergence of damage field, **if a large jump of crack**
 414 **occurs. The reason is multi-fold. First, due to the jump of crack,**
 415 **the displacement solution is far from the current estimate, this**
 416 **challenges the standard Newton procedure. Second, as mention**
 417 **previously, the splitting of the strain energy increases the non-**
 418 **linearity of the problem. Even if the damage field remains stable,**
 419 **numerous iterations are still needed. In addition, a large crack may**
 420 **lead to ill-conditioned mechanical systems**, the integration of the dam-
 421 age update can strongly perturb the mechanical convergence. Numerically,
 422 small damage variations can lead to a significant change of mechanical state.
 423 From a physical point of view, the total dissipated energy in a **discontinuous**
 424 **cracking** step should be larger than the amount due to the crack growth.
 425 Therefore, the crack stability may be reached before the system falls into its
 426 equilibrium state. In order to solve the convergence problem, especially for
 427 the mechanical equilibrium, a semi-implicit scheme is proposed.

428 3.4. A semi-implicit scheme

429 The basic idea is to start with a purely implicit solution for the damage
 430 prediction, and then switch to an explicit solution once the damage con-
 431 verged. As mentioned earlier, many iterations are required for the mechanical
 432 equilibrium after the damage convergence, and the decoupling of these two
 433 problems should help to accelerate this procedure. Therefore, appropriate
 434 convergence criteria are needed for detecting the instabilities as well as the
 435 convergence of each problem (mechanical and damage). We can summarize
 436 the solution scheme as follows:

- 437 • At time step t , $\mathbf{u}^0 = \mathbf{u}_{t-1}$, $d^0 = d_{t-1}$
- 438 • **Mechanical Newton loop** on $i = 0, 1, 2, \dots$
 - 439 1. **Compute a displacement increment** $\delta \mathbf{u}^{i+1} = -\mathbf{K}_u^{-1} \mathbf{R}^u(\mathbf{u}_{t-1}, d^i, t)$
 - 440 2. **Update** $\mathbf{u}^{i+1} = \mathbf{u}_{t-1} + \delta \mathbf{u}^{i+1}$ **and internal variables**

441 3. **Loop for the damage problem: find d by minimizing $\mathbf{R}^d(\mathbf{u}^{i+1}, d)$**
442 **with $\dot{d} \geq 0$**
443 4. Update the damage field: $d^{i+1} = d$
444 5. Convergence check:
445 If $\|d^{i+1} - d^i\| > \epsilon_d$ and $\|\mathbf{R}^u(\mathbf{u}^{i+1}, d^i, t)\| > \epsilon_u$, then $(\cdot)^i \leftarrow (\cdot)^{i+1}$,
446 return to step 1 for next iteration.
447 If $\|d^{i+1} - d^i\| \leq \epsilon_d$ and $\|\mathbf{R}^u(\mathbf{u}^{i+1}, d^i, t)\| \leq \epsilon_u$, then $(\cdot)_t = (\cdot)^{i+1}$,
448 pass to next time step.
449 If $\|d^{i+1} - d^i\| \leq \epsilon_d$ and $\|\mathbf{R}^u(\mathbf{u}^{i+1}, d^i, t)\| > \epsilon_u$, then $d_t = d^{i+1}$, end
450 of iterations and pass to the explicit solution step.

- 451 • Explicit solution at the constant damage d_t : **find \mathbf{u} by minimizing**
452 **$\mathbf{R}^u(\mathbf{u}, d_t, t)$**
- 453 • **If convergence, then $\mathbf{u}_t = \mathbf{u}$, pass to next time step and start**
454 **from the implicit loop**

455 **Contrarily** **Contrary** to purely explicit schemes, the semi-implicit solu-
456 tion is obtained at a converged damage state. Hence, **some** characteristics
457 (e.g. **large** time steps) of the implicit scheme are conserved in this semi-
458 implicit method. In the meantime, the explicit solution at a constant damage
459 allows to efficiently overcome the **difficulties** due to the discontinuous prop-
460 agation. This will be illustrated in numerical experiments with comparison
461 to the modified implicit method.

462 Remark that the solution schemes presented in this section are indepen-
463 dent of the irreversibility implementation. They can be used for any stag-
464 gered phase field model.

465 3.5. Discussion on the accuracy of different solution schemes

466 **Assuming the spatial discretization error is small enough, a nec-**
467 **essary condition to accurate solutions is full-filling the convergence**
468 **criteria for both mechanical and damage problems: $\mathbf{R}^u = 0$ and**
469 **$\mathbf{R}^d = 0$ for $\dot{d} > 0$ and $\mathbf{R}^d > 0$ for $\dot{d} = 0$.**

470 **As shown previously, the explicit schemes only update displace-**
471 **ment and damage fields at staggered steps. The convergence crite-**
472 **ria on $\mathbf{R}^u(\mathbf{u}, d, t)$ and $\mathbf{R}^d(\mathbf{u}, d)$ are never strictly verified . In general,**
473 **explicit schemes only approximate the accurate solutions with suf-**
474 **ficiently small time steps.**

475 Fully implicit schemes, both alternate minimization and the
 476 modified one-loop scheme, should be able to provide accurate re-
 477 sults as they can strictly full-fill the necessary condition at each
 478 time step.

479 The semi-implicit scheme can be regarded as a trade-off between
 480 them. At each time step, the scheme starts from a purely implicit
 481 solution, but activates an explicit solution as long as the damage
 482 field is converged. In discontinuous cracking steps, the converged
 483 solution always verifies the $R^u(\mathbf{u}, d, t) = 0$, but not necessarily the
 484 one on $R^d(\mathbf{u}, d)$. Indeed, the explicitly computed displacement may
 485 introduce a new energy state that can affect the previously com-
 486 puted damage field. However, the influence is expected to be small
 487 and limited, since the semi-implicit solution is obtained with a con-
 488 verged damage field at each time step. In other words, the criterion
 489 on $R^d(\mathbf{u}, d)$ is expected to be verified if the damage field has well
 490 converged. The semi-implicit solution should globally approximate
 491 the accurate fully implicit solution. In particular, we have the fol-
 492 lowing result.

493 **Proposition 1.** *If the explicit and implicit solutions can both converge to the*
 494 *exact solution with time refinement, then the semi-implicit solution converges*
 495 *to the exact solution with time refinement.*

Proof. Let $u \in V \subset H^1(\Omega)$ denote the exact solution, $u_h \in V_h \subset H^1(\Omega)$
 the discretized one. u_h^{Expl} , u_h^{Impl} , $u_h^{\text{Semi-Impl}}$ are defined to be the solutions
 computed respectively by the explicit, implicit and semi-implicit schemes for
 the same spatial and time discretization h . Assuming $u \neq 0$, the following
 relation can be obtained by Hölder's inequality

$$\begin{aligned}
 \sum_{t=1}^n \|u_h(t) - u(t)\|_{L^1(\Omega)} &= \sum_{t=1}^n \left\| \left(\frac{u_h(t)}{u(t)} - 1 \right) u(t) \right\|_{L^1(\Omega)} \\
 &\leq \left\| \left(\frac{u_h(t)}{u(t)} - 1 \right) \right\|_{L^2(\Omega \times \Omega_T)} \|u(t)\|_{L^2(\Omega \times \Omega_T)} \\
 &\leq C_h \|u(t)\|_{L^2(\Omega \times \Omega_T)}
 \end{aligned} \tag{27}$$

where we introduce an error discrepancy factor C_h which only depends on the
 discretization factor h , Ω_T denotes the time domain. Assuming the spatial
 discretization error is neglectable, the convergence of u_h with respect to time

refinement is defined as: $\lim_{h \rightarrow 0} C_h = 0$. Hence, the convergence of explicit and implicit solutions can be defined as

$$\begin{aligned} \sum_{t=1}^n \|u_h^{\text{Expl}}(t) - u(t)\|_{L^1(\Omega)} &\leq C_h^1 \|u(t)\|_{L^2(\Omega \times \Omega_T)} \\ \sum_{t=1}^n \|u_h^{\text{Impl}}(t) - u(t)\|_{L^1(\Omega)} &\leq C_h^2 \|u(t)\|_{L^2(\Omega \times \Omega_T)} \end{aligned} \quad (28)$$

By definition, we have

$$\begin{aligned} \sum_{t=1}^n \|u_h^{\text{Impl}}(t) - u(t)\|_{L^1(\Omega)} &\leq \sum_{t=1}^n \|u_h^{\text{Semi-Impl}}(t) - u(t)\|_{L^1(\Omega)} \\ &\leq \sum_{t=1}^n \|u_h^{\text{Expl}}(t) - u(t)\|_{L^1(\Omega)} \end{aligned} \quad (29)$$

Therefore, if $\lim_{h \rightarrow 0} C_h^1 = 0$ and $\lim_{h \rightarrow 0} C_h^2 = 0$, then

$$\lim_{h \rightarrow 0} \sum_{t=1}^n \|u_h^{\text{Semi-Impl}}(t) - u(t)\|_{L^1(\Omega)} = 0 \quad (30)$$

496 Analogically, the above equality holds for $u = 0$. The proof is closed. \square

497 3.6. Implementation in Cast3M

498 The proposed method can be easily implemented in the code Cast3M
 499 without supplementary developments. Particularly, the material behavior
 500 generator MFront [41] is used here for implementing the softening mechan-
 501 ical response due to the cracking. For summarizing, the overall phase field
 502 algorithmic implementation is illustrated in Algorithm 1. In addition, this
 503 work makes use of the convergence acceleration tools available in Cast3M,
 504 i.e. the fix point acceleration techniques [39], when solving the mechanical
 505 problem.

506 3.7. Discussion on the choice of convergence *criteria*

507 The proposed semi-implicit solution scheme requires several convergence
 508 checks. Generally speaking, different criteria can be used. For example,
 509 for the mechanical loop, we can check also the convergence on displacement

Algorithm 1: Semi-implicit staggered phase field implementation

Input: Solution at previous instant: $\mathbf{u}_{t-1}, d_{t-1}$

Output: Solution at current instant: \mathbf{u}_t, d_t

```
1 Initiation:  $\delta\mathbf{u}^0 = 0, \delta d^0 = 0$ 
2 for  $i = 0, \dots, i_{\max}$  do
3   Compute a displacement increment:  $\delta\mathbf{u}^{i+1}$ 
4   Update displacement:  $\mathbf{u}^{i+1}$ 
5   Update and internal variables:  $\boldsymbol{\sigma}, \psi_e^+$  // via MFront
6   Update damage variable:  $d^{i+1}$  // Algorithm 2
   /* Check convergence: */
7   if  $\|d^{i+1} - d^i\| \leq \epsilon_d \ \& \ \|\mathbf{R}^u(\mathbf{u}^{i+1}, d^i)\| \leq \epsilon_u$  then
8      $(\cdot)_t \leftarrow (\cdot)^{i+1}$ 
9     End Loop
10  else if  $\|d^{i+1} - d^i\| \leq \epsilon_d \ \& \ \|\mathbf{R}^u(\mathbf{u}^{i+1}, d^i)\| > \epsilon_u$  then
11     $d_t \leftarrow d^{i+1}$ 
12    Solve  $\mathbf{u}_t$  at constant damage  $d_t$  // Algorithm 3
13    End Loop
14  else
15     $(\cdot)^i \leftarrow (\cdot)^{i+1}$ 
16 Return  $\mathbf{u}_t, d_t$ 
```

510 variation: $\|\delta\mathbf{u}^{i+1}\|$ in addition to the global equilibrium $\mathbf{R}^u = 0$, or just use
511 one of these two criteria instead. **In principle, the global equilibrium**
512 **ensures automatically the convergence on displacement variation.**
513 **Conversely, it is not true.** The influence of different criteria on computa-
514 tional cost can be studied, but is out of the scope of this work. In any cases,
515 the relative tolerance for **mechanical and damage** convergence check, **re-**
516 **spectively related to ϵ_u and ϵ_d** (Algorithm 1 and 3), should be at least
517 of order 10^{-4} for a good accuracy. The **irreversibility** tolerance ϵ_c used
518 in Algorithm 2 should be at least of order 10^{-2} . In the following numerical
519 examples, both displacement stability and equilibrium residual are used for
520 the mechanical convergence. The damage convergence is considered by the
521 crack stability, as shown in the algorithms.

Algorithm 2: Phase field solution under irreversibility condition

Input: Solution at previous instant: d_{t-1} , reference energy: ψ_e^+

Output: Damage prediction: d

```
1 Initiation:  $p(x) = 0, \forall x \in \Omega, \mathcal{D} = \emptyset$ 
2 for  $i = 1, \dots, i_{\max}$  do
3   Compute  $d^i$  with  $p$  and  $d^i = d_{t-1}$  on  $\mathcal{D}$  // Equation (26)
4   Detect new constraint set:  $\mathcal{D}^* = \{x \in \Omega \mid d^i < d_{t-1}\}$ 
   /* Check convergence: */
5   if  $\mathcal{D}^* = \emptyset$  or  $\|d^i - d^{i-1}\|_{\infty} \leq \epsilon_c$  then
6      $d = d^i$ 
7     End Loop
8   else
9     Update the constraint set  $\mathcal{D} = \mathcal{D} \cup \mathcal{D}^*$ 
10    Update the indicator function  $p(x) = 1, \forall x \in \mathcal{D}$ 
11     $(\cdot)^{i-1} \leftarrow (\cdot)^i$ 
12 Return  $d$ 
```

Algorithm 3: Explicit solution under constant damage

Input: Solution at previous instant: \mathbf{u}_{t-1} , constant damage: d_t

Output: Solution at current instant: \mathbf{u}_t

```
1 Initiation:  $\delta \mathbf{u}^0 = 0$ 
2 for  $i = 0, \dots, i_{\max}$  do
3   Solve the mechanical problem with  $d_t$ :  $\delta \mathbf{u}^{i+1}$ 
4   Update displacement:  $\mathbf{u}^{i+1}$ 
5   Update internal variables:  $\boldsymbol{\sigma}$  // via MFront
   /* Check convergence: */
6   if  $\|\mathbf{R}^u(\mathbf{u}^{i+1}, d_t)\| \leq \epsilon_u$  then
7      $(\cdot)_t \leftarrow (\cdot)^{i+1}$ 
8     End Loop
9   else
10     $(\cdot)^i \leftarrow (\cdot)^{i+1}$ 
11 Return  $\mathbf{u}_t$ 
```

522 **4. Numerical experiments**

523 *4.1. Single edge notched tensile test*

524 The first test concerns the well known single edge notched tensile test
525 [10]. Figure 2 illustrates the geometry and prescribed boundary conditions.
526 The displacement loading is imposed on the top side of the specimen while
527 keeping the bottom side fixed. The material properties are set to the same
528 as [10]: Young’s modulus $E = 210 \text{ kN/mm}^2$, Poisson’s ratio $\nu = 0.3$, critical
529 energy release rate $G_c = 2.7 \times 10^{-3} \text{ kN/mm}$. The FE mesh is generated using
530 linear triangular elements and refined around the expected crack path for a
531 size about twice smaller than the concerned regularization length.

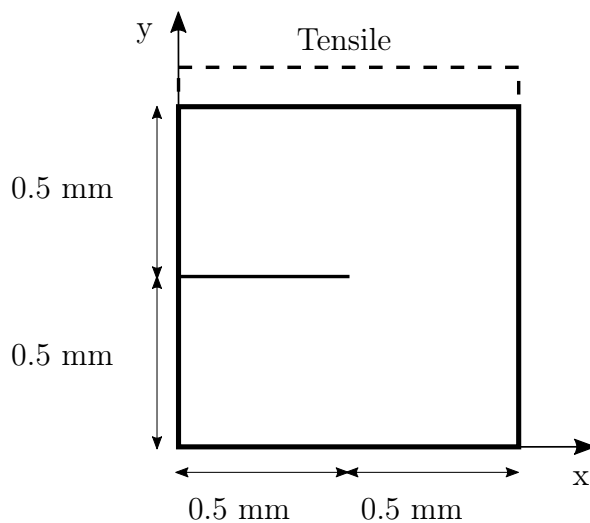


Figure 2: Geometry and boundary conditions for single edge notched test [mm]

532 *4.1.1. Comparison of different irreversibility implementations*

533 In order to demonstrate the capability of the proposed irreversibility im-
534 plementation, we compare three different methods: the method introducing
535 \mathcal{H} [10] (referred to as \mathcal{H} -model), standard Lagrangian method [28] (referred
536 to as variational model), and the proposed method of this work. Particularly,
537 the explicit solution scheme is employed here for its robustness to discontin-
538 uous crack propagation. In the following experiments, relatively fine loading
539 steps have to be used, which are considered as follows: $\delta u = 6.71 \times 10^{-5} \text{ mm}$
540 for the first 80 steps, then $\delta u = 6.71 \times 10^{-6} \text{ mm}$. **The Lagrangian method**
541 **is implemented in Cast3M using an active-set method.**

542 Figure 3 illustrates the crack patterns for different models. Due to the loss
 543 of equivalence to the original variational formulation, the \mathcal{H} -model leads to a
 544 crack profile different from the variational model. Although the crack length
 545 at the current loading stage is overall the same in this example, this difference
 546 in crack profiles shows that the different models can result in **completely**
 547 **different cracking behaviors** **different numerical behaviors and po-**
 548 **tentially lead to different local minima and convergence rates.** As
 549 expected, the proposed method can produce a very similar result to the vari-
 550 ational model, which confirms the equivalence between them. However, the
 551 proposed method is much more efficient than the variational model using the
 552 existing implementation for the variational inequality, as shown in Table 1.

553 We remark here that the validity of these solutions is out of the scope
 554 of this discussion. For obtaining a realistic crack pattern with an explicit
 555 scheme, a much finer time discretization is needed. However, this is not a
 556 problem for the comparison of different **numerical** behaviors conducted by
 557 different phase field models. **The use of explicit scheme is for the pur-**
 558 **pose of giving similar constant input energies to different models**
 559 **at each time step.**

560 At the end of the first comparison, we illustrate additionally the numerical
 561 dissipation energy of the proposed model during the crack propagation (see
 562 Figure 4). The dissipation is computed as follows

$$\hat{G}_c = \frac{\delta(\Pi_{\text{ext}} - \Pi_e)}{2\delta \text{ crack length}} \quad (31)$$

563 we recall that Π_{ext} and Π_e stand for the external work and the elastic energy
 564 stored in the cracked body respectively. In a continuous cracking step, the nu-
 565 merical dissipation should be equal to the theoretical one that is prescribed in
 566 the phase field formulation. As shown in the figure, the initiation of cracking
 567 needs a much higher energy. Then, due to the **discontinuous** crack propa-
 568 gation, the computed dissipation differs significantly from the theoretical one
 569 at the beginning of propagation. As the cracking becomes continuous, the
 570 numerical dissipation converges to the theoretical reference. This confirms
 571 the energetic aspect of the proposed irreversibility implementation.

572 4.1.2. Comparison of different solution schemes

573 In the second part of this test-case, we compare different solution schemes:
 574 explicit, implicit (the modified one) and semi-implicit schemes. The proposed
 575 irreversibility implementation is adopted, as an alternative implementation

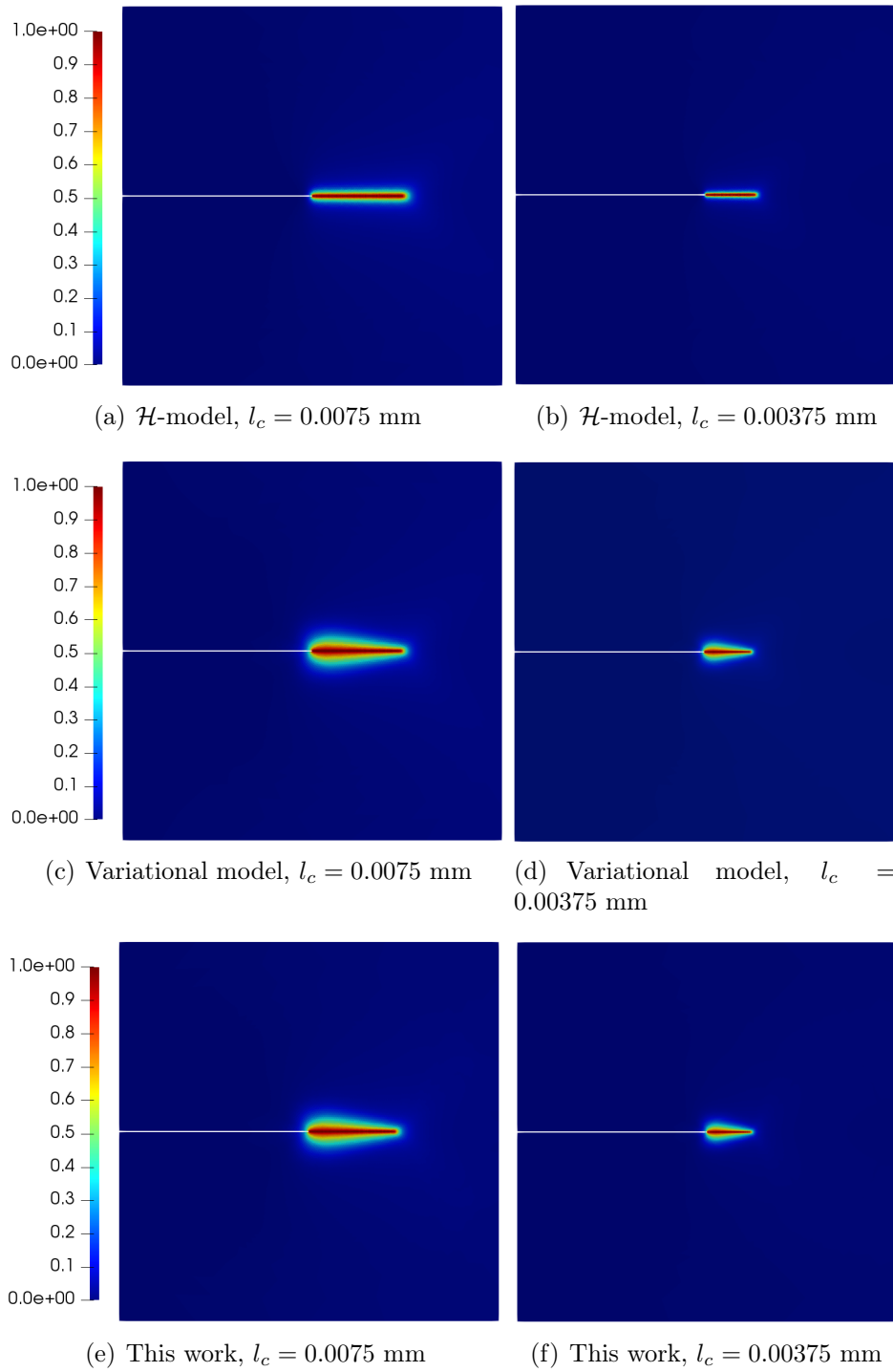


Figure 3: Crack patterns at $u = 6.71 \times 10^{-3}$ mm provided by the explicit solution scheme for different models

Table 1: Computational cost for different models in the tensile test

Model	Solver	l_c (mm)	CPU Time
Variational model	Expl.	0.0075	225 min
		0.00375	703 min
This work	Expl.	0.0075	55 min
		0.00375	160 min

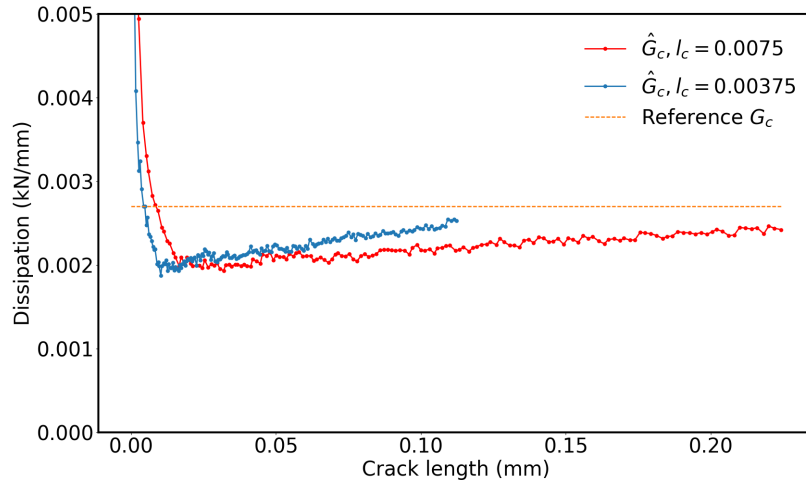


Figure 4: Numerical dissipation during the crack propagation with the proposed irreversibility implementation

576 for the variational inequality. The internal characteristic length $l_c = 0.015$
577 mm is used here. The loading increment is considered as follows: $\delta u =$
578 6.1×10^{-4} mm for the first 8 steps, $\delta u = 6.1 \times 10^{-5}$ mm for the remaining 20
579 steps until $u = 6.1 \times 10^{-3}$ mm. It should be noticed that these loading steps
580 are usually considered too large for an explicit solution in such experiments.
581 Suitable loading steps for accurate explicit solutions should be at the most
582 of the order of 10^{-6} mm [10].

583 As shown in Figure 5, these loading steps are too large for an explicit
584 scheme. The final crack patterns are strongly dependent of the time dis-
585 cretization. For obtaining a full crack, the loading steps have indeed to be
586 100-times smaller. On the contrary, the implicit scheme does not impose such
587 requirement for the loading steps. The full crack is obtained without refining
588 time discretization. The proposed semi-implicit scheme has similar proper-
589 ties. Figure 6 illustrates the crack evolution in the specimen. It is shown that
590 the crack initiates around $u = 5.612 \times 10^{-3}$ mm and goes through the entire
591 specimen within one time step. This discontinuous propagation appears in
592 explicit solutions only when the time step decreases sufficiently. We can see
593 that the final crack pattern is completely independent of loading steps **with**
594 **the semi-implicit method** in this example. Larger loading steps can be
595 used without perturbing the final crack pattern.

596 **However, if we take a look at Figure 7, the reaction force is**
597 **still sensible to the time discretization, even with implicit or semi-**
598 **implicit schemes. In order to have a good representation of loading**
599 **history, the time steps should not be too large. In general, semi-**
600 **implicit solutions should converge with time refinement at a better**
601 **rate than explicit solutions. Taking the maximal reaction force of**
602 **the implicit solution as a reference, we can illustrate the conver-**
603 **gence trends (see Figure 8). It is shown that the semi-implicit**
604 **solutions converge much faster than the explicit solutions by refin-**
605 **ing the time steps.**

606 In this example, the discontinuous propagation causes a sudden drop of
607 external forces and **a big jump of state** on displacement field. Therefore,
608 numerous iterations are needed to find **mechanical** equilibrium, and some-
609 times, no convergence can be found within a limited time with the purely
610 implicit scheme.

611 The semi-implicit scheme is notably more efficient than the implicit one.
612 As shown in Table 2, the semi-implicit solutions take only several hours in
613 this experiment, whereas the implicit solutions encounter severe difficulties

614 of convergence and need more than 20 hours to find global mechanical
615 equilibrium. This implicit scheme is able to bypass the discontinuous
616 cracking step with numerous iterations, but still hardly converges in the following steps. This happens as well in other
617 experiments, this point will be more discussed in the second example. The semi-implicit scheme is able to overcome these difficulties
618 by fixing the damage variable. For the same reason, explicit solutions are also very robust for the discontinuous crack propagation. However, as
619 shown in Table 2, the computational cost of explicit solutions increases exponentially as the time step decreases and can rapidly become un-affordable
620 if a high accuracy of results is demanded.
621
622
623
624

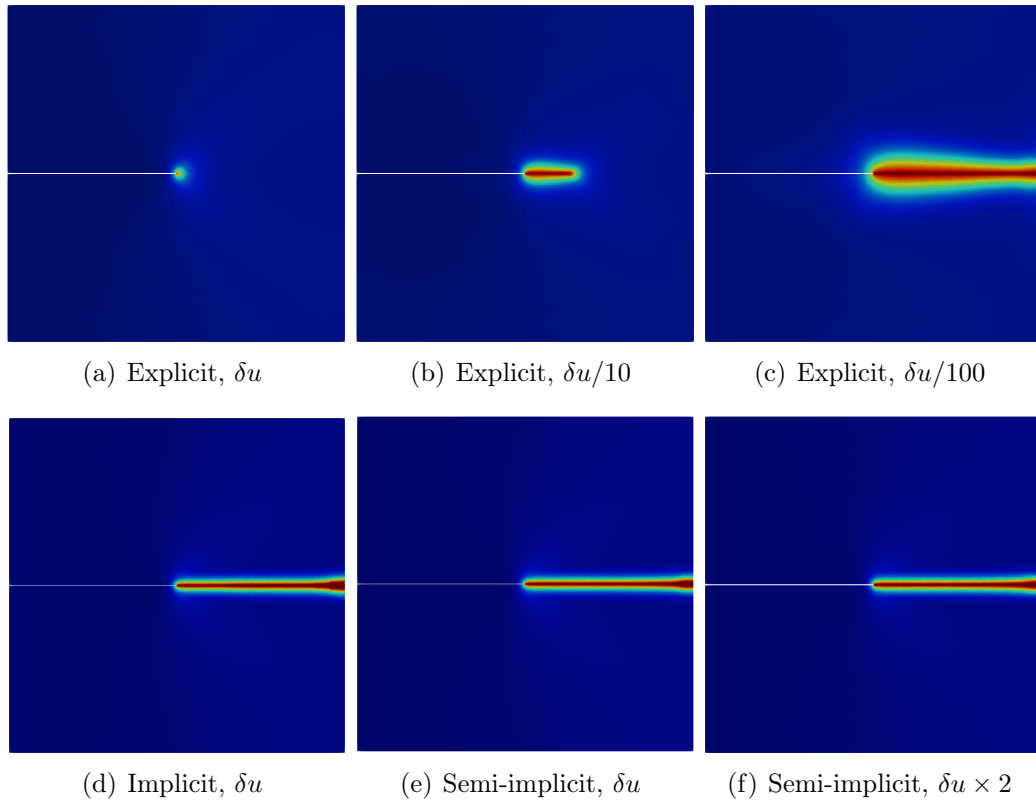


Figure 5: Final crack patterns in the single edge notched tensile test with different solution schemes

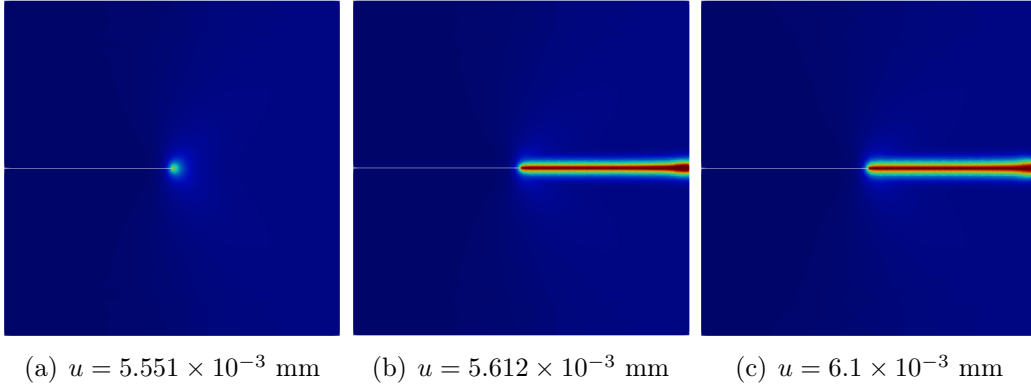


Figure 6: Discontinuous crack evolution in the single edge notched tensile test

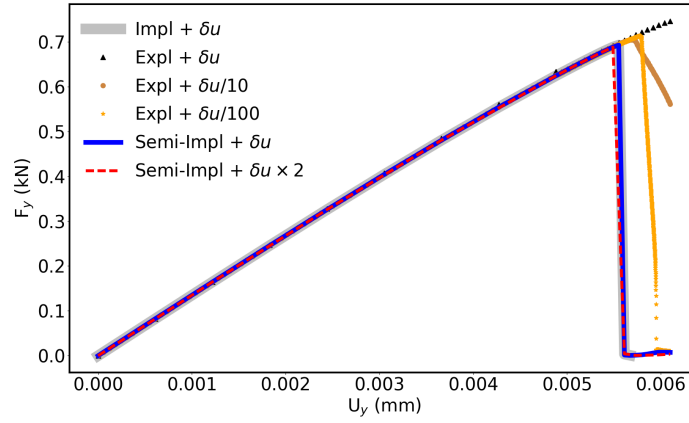


Figure 7: Evolution of reaction force in the single edge notched tensile test

Table 2: Computational cost for the single edge notched tensile test

Model	Solver	Step size	Full crack	Iterations	CPU Time
This work	Expl.	δu	No	229	2 min
		$\delta u/2$	No	756	4 min
		$\delta u/10$	No	6462	43 min
		$\delta u/100$	Yes	97691	506 min
	Impl.	δu	Yes	-	>1000 min
	Semi-impl.	δu	Yes	17467	348 min
		$\delta u \times 2$	Yes	14329	306 min

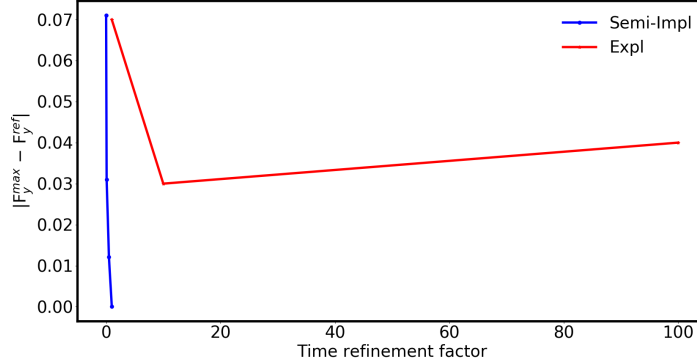


Figure 8: Convergence studies with respect to time step refinement

625 *4.2. Asymmetric double notched tensile specimen*

626 The second experiment consists in the well studied asymmetric double
627 notched specimen [42, 27, 43]. Figure 9 illustrates the geometry and pre-
628 scribed boundary conditions. The used materials properties are the same as
629 [27]: $E = 210 \text{ kN/mm}^2$, $\nu = 0.3$, $G_c = 2.7 \times 10^{-3} \text{ kN/mm}$, $l_c = 0.2 \text{ mm}$. The
630 FE mesh is generated using linear triangular elements and refined around
631 the expected crack paths for a mesh size up to 0.1 mm , which is twice infe-
632 rior to the internal characteristic length l_c . This model contains 26297 nodes
633 and 52520 elements. The displacement increment is considered as follows:
634 $\delta u = 5.01 \times 10^{-3} \text{ mm}$ for the first 8 steps, $\delta u = 5.01 \times 10^{-4} \text{ mm}$ for the
635 remaining 20 steps until $u = 5.1 \times 10^{-2} \text{ mm}$.

636 Figure 10 illustrates the crack evolution obtained with the proposed phase
637 field implementation and semi-implicit scheme. The final crack pattern shows
638 an excellent agreement with the experimental observation in many brittle ma-
639 terials [43]. **Similar numerical results can be obtained with explicit**
640 **schemes using small time steps, as reported in [27]. Physically,**
641 **this repulsive behavior of two parallel cracks is completely possible**
642 **within linear elastic fracture mechanics theory, as explained by the**
643 **work [43], although the attraction or repulsion depends strongly on**
644 **the geometry condition of the two approaching cracks. One expla-**
645 **nation is that the propagation direction is altered by the interaction**
646 **between the stress fields around the crack tips, as they get closer.**
647 **The crack angle θ with respect to initial direction intends to pro-**
648 **mote the pure opening mode, i.e. stress intensity factor $K_{II}(\theta) = 0$.**

649 Interested readers can refer to [43] for more details.

650 In the numerical experiment, initial cracks start propagating
651 around $u = 4.11 \times 10^{-2}$ mm and the en passant cracks appear within
652 one time step. This discontinuous propagation requires many iterations
653 for the convergence of solutions, as shown in Figure 11. Figure 11(a) depicts
654 the iteration numbers of each time step with the one-loop implicit
655 and the semi-implicit schemes. The most difficult time step for the im-
656 plicit scheme turns out to be the one (step 11) right after the discontinuous
657 cracking. This may be explained by the fact that the system becomes highly
658 nonlinear with respect to the displacement due to the splitting of
659 strain energy and ill-conditioned with a large crack. The strong
660 coupling of displacement and damage fields amplifies the perturba-
661 tion of damage variation on the mechanical convergence. Experience
662 shows that even small variations in the damaged region can severely perturb
663 the iterative Newton procedure. As shown in Figure 11(b), the mechanical
664 problem converges very slowly with the purely implicit scheme, despite of
665 the globally stable damage field. However, by decoupling the mechanical
666 and damage problems and considering that the damage solution has been
667 found, the solution can quickly converge to a local minimum. This is
668 shown by the excellent convergence behavior of the semi-implicit solution.

669 Table 3 summarizes the computational cost for different solution cases.
670 The implicit scheme did not converge after a long time for the discontinuous
671 cracking steps. It is shown that the semi-implicit scheme is much more
672 robust and efficient than the purely implicit scheme with a significant speed-
673 up.

Table 3: Computational cost for the double notched tensile test

Model	Solver	Iterations	CPU Time
This work	Impl.	>17685	>1000 min
	Semi-impl.	7673	269 min

674 4.3. Symmetric three points bending test

675 Next, we investigate the performance of proposed methods in a different
676 loading case. The symmetric three points bending test is used (see Fig-
677 ure 12). In order to avoid the damage around the loading points, a small
678 region closed to the loading is considered purely elastic, while the remaining

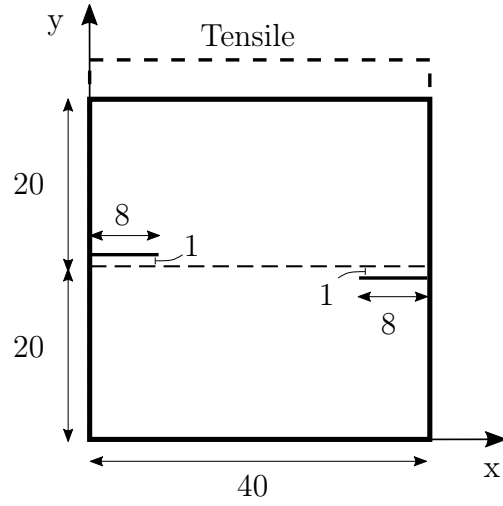


Figure 9: Geometry and boundary conditions for double notched tensile specimen [mm]

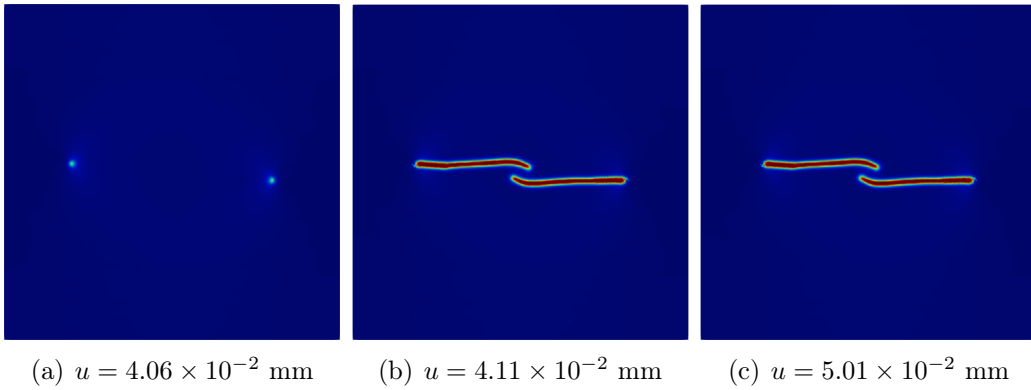
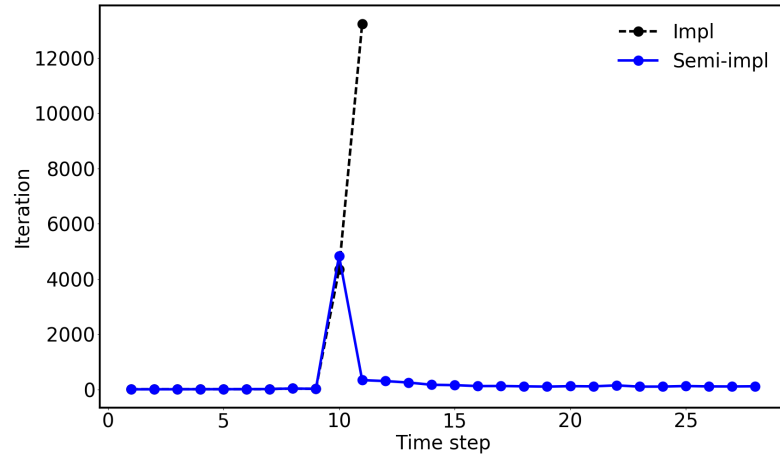
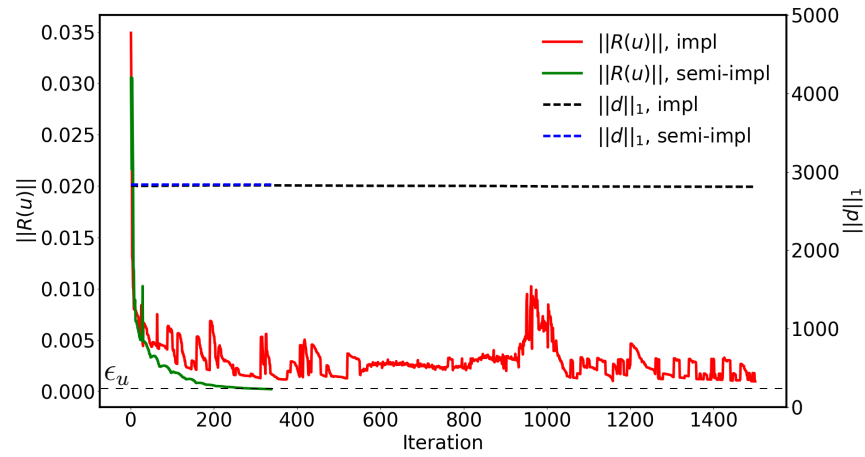


Figure 10: Crack evolution in the double notched tensile specimen



(a) Iteration number per time step



(b) Iterative residual in the step t_{11}

Figure 11: Iteration number and iterative residual

679 part of specimen is considered damageable. The used materials properties
680 are the same as [10]: $E = 20.8 \text{ kN/mm}^2$, $\nu = 0.3$, $G_c = 5 \times 10^{-4} \text{ kN/mm}$.
681 The mesh is refined around the expected crack path. The resulting FE model
682 contains 19694 triangular elements. Taking advantage of the semi-implicit
683 scheme, a uniform large displacement increment is used: $\delta u = 6 \times 10^{-3} \text{ mm}$.
684 Figure 13 shows the evolution of crack for a maximum displacement loading
685 $u = 6 \times 10^{-2} \text{ mm}$. As expected, the crack grows vertically and stops near the
686 elastic region. Figure 13 shows the crack evolution for two internal lengths.
687 **Similar results have been reported in the literature (see e.g. [10]).**
688 **In our numerical experiments, a smaller internal length leads to**
689 **stronger numerical instabilities, which causes therefore a higher**
690 **computational cost (see Table 4). One of the reasons may relate**
691 **to the mesh size effect, as the mesh becomes closer to the internal**
692 **length when decreasing the latter. Regardless of the strong nu-**
693 **merical instabilities, the semi-implicit scheme is able to converge**
694 **at a limited time cost.**

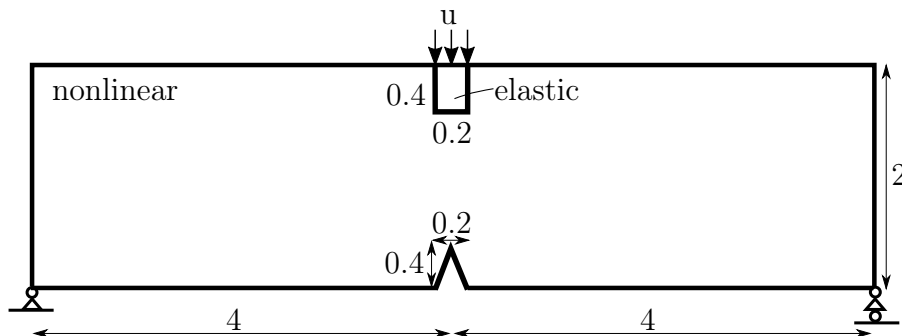


Figure 12: Geometry and boundary conditions for three points bending test [mm]

Table 4: Computational cost for the bending test

Model	Solver	L_c (mm)	Iterations	CPU Time
This work	Semi-impl.	0.06	6653	137 min
		0.03	70959	780 min

695 4.4. Crack nucleation and propagation in a two-phase concrete material

696 Then, we consider a heterogeneous specimen. Figure 14 illustrates a two-
697 phase simplified concrete material without any initial crack. Particularly,

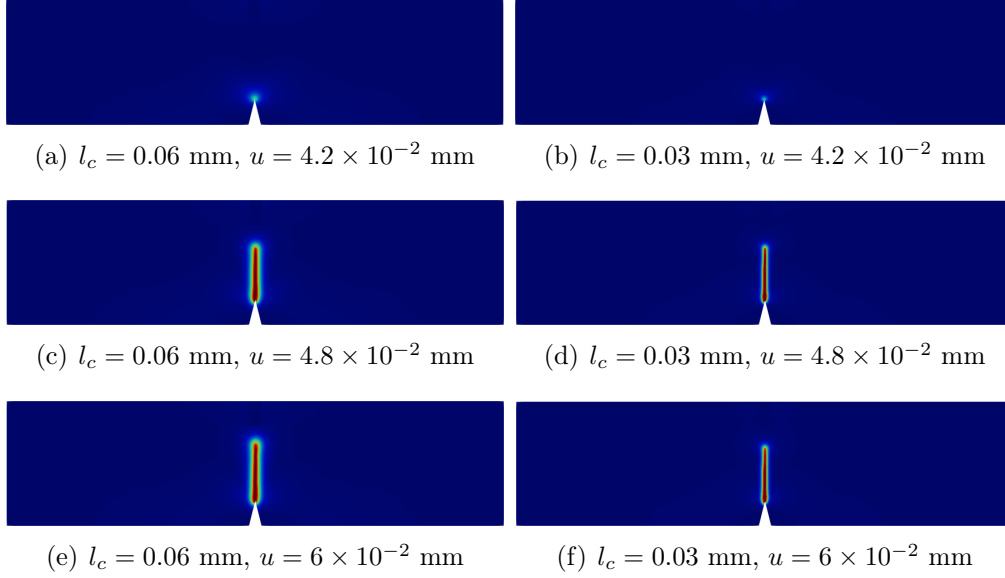


Figure 13: Crack evolution in the three points bending test

698 the inclusions are considered purely elastic with $E = 100$ kN/mm², $\nu = 0.2$.
 699 **Hence, no damage equations are solved within the inclusion phase.**
 700 The matrix is considered damageable with the following properties: $E = 20$
 701 kN/mm², $\nu = 0.3$, $G_c = 5 \times 10^{-5}$ kN/mm, $l_c = 0.025$ mm. A displacement
 702 loading is applied on the top side, while the bottom side is fixed. The FE
 703 mesh is generated using triangular elements for a uniform size of 0.017 mm.
 704 This results in 88241 elements. The proposed phase field implementation is
 705 used with three different large uniform loading steps: $\delta u = 1 \times 10^{-3}$ mm,
 706 $\delta u/5$, and $\delta u/10$.

707 Figure 15 illustrates the final crack patterns obtained with different load-
 708 ing steps. The evolution of the reaction forces is shown in Figure 16. In
 709 this example, a loading step dependency is observed. This is associated
 710 with the intrinsic history-dependence nature of the underlying fracture prob-
 711 lem. In previous examples, where the materials are considered homogeneous,
 712 stresses induced by the applied loading are uniform and monotonically in-
 713 crease. Therefore, we can adopt large time steps without modifying final
 714 crack patterns, **using the implicit or** semi-implicit schemes. However, this
 715 is not the case for this heterogeneous material, loading steps have to be care-
 716 fully chosen for accurately representing the loading history. Numerically, it
 717 can be noticed that the irreversibility condition is implemented in a time-

718 discrete manner. ~~which clearly shows the history-dependence nature~~
 719 ~~of the underlying problem. We remark that this dependency is~~
 720 ~~true for any kind of solution schemes. The semi-implicit scheme~~
 721 ~~can accept relatively larger time steps in any cases, compared to~~
 722 ~~explicit ones.~~ This example emphasizes the adequate choice of time
 723 steps, even with the implicit or the proposed semi-implicit schemes.
 724 However, we can expect better convergence rates against the ex-
 725 plicit schemes. Indeed, explicit schemes have been tested with the
 726 finest time steps: $\delta u/10$, the solution is far from convergence.

727 The computational cost of each solution is summarized in Table 5. This
 728 shows again the efficiency of the proposed phase field implementation.

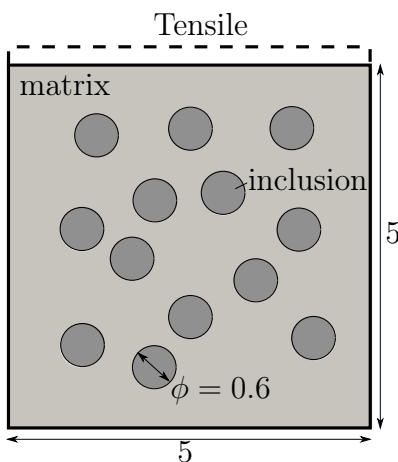


Figure 14: Geometry and boundary conditions for the two-phase concrete material [mm]

Table 5: Computational cost for the two-phase concrete specimen

Model	Solver	Step size	Iterations	CPU Time
This work	Semi-impl.	δu	1002	132 min
		$\delta u/5$	4344	391 min
		$\delta u/10$	8649	387 min

729 *4.5. Thermal shock test*

730 The final test concerns a thermal shock problem [44, 45], which is well
 731 studied both experimentally and analytically. The geometry and boundary

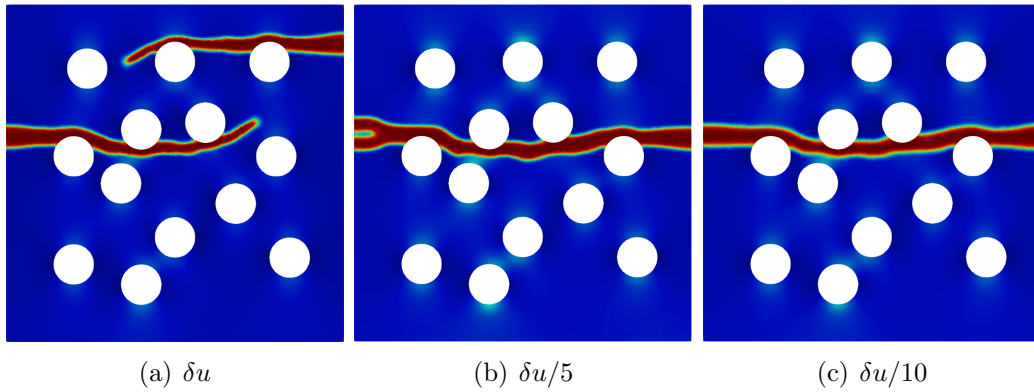


Figure 15: Final crack patterns of the concrete material obtained with different step sizes.

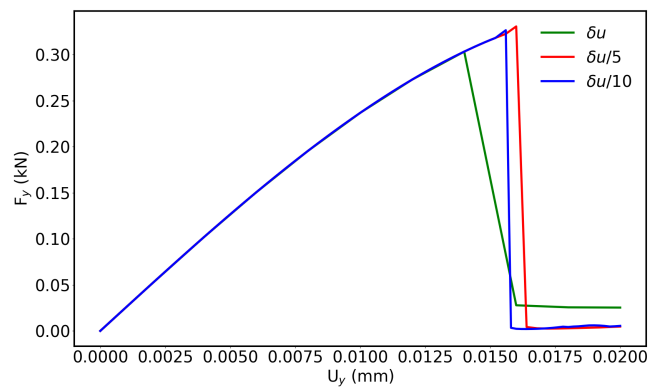


Figure 16: Evolution of the reaction force in the concrete material

732 conditions for numerical analysis is illustrated in Figure 17. The plate is
 733 initially subjected to a uniform temperature T_0 . From time $t > 0$, a colder
 734 temperature T_1 is prescribed on the upper side. All the exposed surfaces are
 735 considered adiabatic. Assuming the length of plate is sufficiently long, the
 736 temperature field at $t > 0$ can be analytically given by

$$T(x, y) = T_0 - (T_1 - T_0)f_c\left(\frac{y}{2\sqrt{k_c t}}\right), \quad \forall t > 0 \quad (32)$$

737 where k_c is the thermal conductivity, f_c is the complementary error function:
 738 $f_c(x) = \frac{2}{\sqrt{\pi}} \int_x^\infty e^{-s^2} ds$. Therefore, the temperature is uniform in the direction
 739 x , while a high temperature gradient appears in the direction y . The elastic
 740 strain induced by the thermal expansion reads then

$$\boldsymbol{\varepsilon}_e = \boldsymbol{\varepsilon} - \boldsymbol{\varepsilon}_{\text{th}} = \boldsymbol{\varepsilon} - \alpha(T - T_0)\mathbf{I} \quad (33)$$

741 where α is the thermal expansion coefficient, \mathbf{I} is the second order identity
 742 matrix.

743 In this work, the loading parameters and material properties are con-
 744 sidered as the same as in [45]. Some important loading parameters and
 745 material properties are given in Table 6. In order to have results comparable
 746 with those reported in [44, 45], we do not differentiate the compression and
 747 traction effect in the phase field model. The FE model is generated using
 748 linear triangular elements with a plane stress assumption. In order to well
 749 represent the thermal shock history, the time steps are considered as follows:
 750 $\delta t = 5 \times 10^{-4}$ for the first two steps, then $\delta t = 1 \times 10^{-3}$ for the remaining
 751 steps.

752 As shown in Figure 18, the crack starts being homogeneous in the direc-
 753 tion parallel to the surface of the thermal shock. At some critical time, the
 754 homogeneous solution bifurcates towards a periodical solution with equal dis-
 755 tance cracks penetrating inside the specimen. The wave length, which stands
 756 for the distance between two neighboring cracks, is initially equal to 7.4 times
 757 of the internal characteristic length. After some time, some cracks stop to
 758 propagate whereas the others continue with a wave length approximately two
 759 times higher than the original one. These results show an excellent agreement
 760 with both analytical analyses [44] and experimental results [45]. In terms of
 761 computational cost, this experiment takes only several hours with the pro-
 762 posed phase field implementation. **However, full Lagrangian methods**
 763 **will take several days for this kind of computations.**

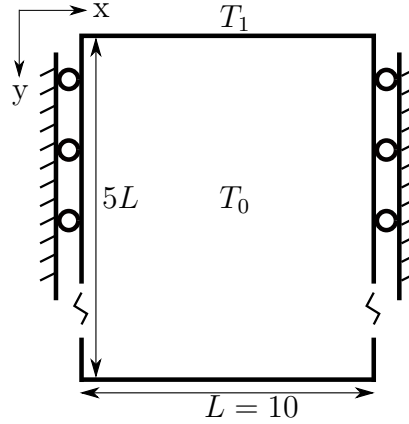


Figure 17: Geometry and boundary conditions for thermal shock test [mm]

Table 6: Loading parameters and material properties for the thermal shock test

T_0 (K)	T_1 (K)	E (GPa)	ν	α (K^{-1})	G_c (kN/mm)
673	293	370	0.22	8.4×10^{-6}	12.16×10^{-6}

764 **5. Conclusion**

765 A novel phase field method for quasi-static brittle fracture analysis has
 766 been developed. This method is based on two novel algorithmic implemen-
 767 tations: a novel efficient algorithm for imposing the irreversibility condition
 768 and a robust staggered semi-implicit solution scheme for overcoming the **dis-**
 769 **continuous** propagation and time step constraints.

770 The irreversibility implementation is based on an efficient implementation
 771 of the inequality constrained optimization procedure with vanishing energetic
 772 driving force. Unlike the \mathcal{H} field based model, the proposed method can keep
 773 the original variational nature of the phase field solution. Moreover, this
 774 method does not introduce any supplementary numerical coefficient which
 775 may result in ill-conditioned systems. This method can be considered as a
 776 variant to conventional variational phase field models.

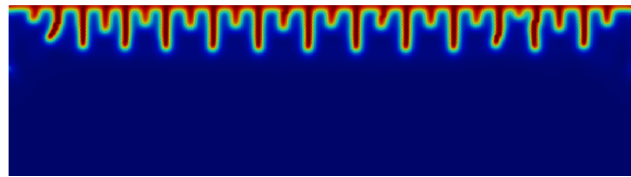
777 The proposed semi-implicit staggered scheme relies on two ingredients:
 778 the integration of phase field solution into the mechanical loop, and the com-
 779 bination of the purely implicit and explicit solution schemes. This method
 780 allows to **alleviate** the time step constraints, while being very robust with
 781 the **numerical instabilities associated with the discontinuous** propa-
 782 gation.



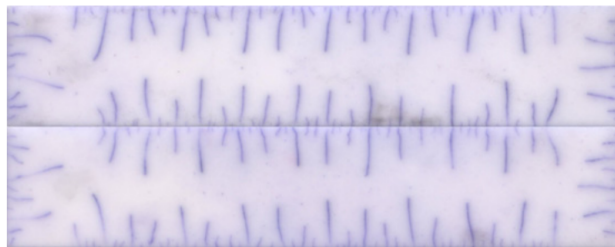
(a) $t = 5 \times 10^{-4}$ s



(b) $t = 1 \times 10^{-3}$ s, wave length $\approx 7.4l_c$



(c) $t = 1.8 \times 10^{-2}$ s, wave length $\approx 15l_c$



(d) Crack pattern on both faces after a thermal shock

Figure 18: Crack evolution in the thermal shock test. (a) (b) (c): Simulated cracks with $l_c = 5 \times 10^{-2}$ mm, (d): Experimental results [45].

783 The proposed phase field method can be easily implemented. Numerical
 784 examples considering different materials, loading cases and geometries have
 785 demonstrated the efficiency and robustness of the proposed method. The
 786 proposed method is expected to provide a novel efficient tool for brittle frac-
 787 ture analysis by phase field methods. Applications of the proposed method
 788 to 3D heterogeneous concrete materials and nuclear fuel elements that are
 789 subjected to a long-term loading (up to years) are ongoing.

790 Acknowledgement

791 This research was conducted in the framework of the ‘PLEIADES‘ project,
 792 which is supported financially by the CEA (Commissariat à l’Energie Atom-
 793 ique et aux Energies Alternatives), EDF (Electricité de France) and Fram-
 794 atome. In addition, the authors would like to acknowledge the financial
 795 support of the Cross-Disciplinary Program on Numerical Simulation of CEA
 796 (PTC FUEL).

797

798 Appendix A. Numerical study of the impact of the irreversibility 799 implementation

800 The important features of the proposed implementation are:
 801 irreversible updating of the constrained set and vanishing energetic
 802 force. The impact of the first feature is easier to see. Due to the
 803 updating strategy, the resulting constraint set may not be optimal
 804 for a given energy state. Consequently, the computed damage field
 805 may be somehow degraded.

806 The impact of vanishing energy is less obvious. Unlike the an-
 807 alytic formulation, the vanishing energy $\psi_e^+ = 0$ can not be directly
 808 imposed with discretized formulation for the constrained nodes,
 809 since the strain energy is usually computed inside an element for
 810 integration points. To do this, a mapping of the energy between its
 811 nodal and element-based values is needed. Denoting by $\mathcal{M} : \mathbb{R} \rightarrow \mathbb{R}$
 812 the mapping from the element-based value to the nodal value, and
 813 \mathcal{M}^{-1} its inverse mapping, the proposed irreversibility implementa-
 814 tion requires first a nodal representation of the strain energy

$$\psi_e^{+nodal} = \mathcal{M}(\psi_e^+) \quad (\text{A.1})$$

815 then applying the vanishing energy condition for constrained set:
 816 $\psi_e^{+nodal}(x) = 0, \forall x \in \mathcal{D}$, the final strain energy used for computing
 817 damage field is obtained by

$$\psi_e^{+*} = \mathcal{M}^{-1}(\psi_e^{+nodal}) \quad (\text{A.2})$$

818 In the above procedure, the mapping introduces naturally an in-
 819 terpolation error, but we can expect this error is controllable by
 820 refining the mesh and choosing appropriate interpolation methods.
 821 When applying the vanishing energy condition to a constrained
 822 point, a part of the reference energy ψ_e^+ will be removed from its
 823 surrounding elements. Hence, the computed damage can be less
 824 important than that of full Lagrangian method.

825 In order to illustrate the impact of the method, let us consider a
 826 1D bar with $G_c = 2.7 \times 10^{-3}$ kN/mm and $l_c = 0.015$ mm. We assume
 827 a piece-wise constant element-based reference energy ψ_e^+ is given
 828 in different time steps. Initially, a predefined crack is computed
 829 with the following energy distribution

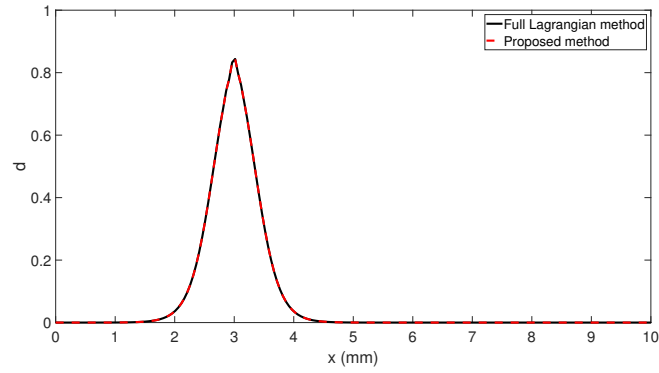
$$\psi_e^+(x, t = 0) = 0.5e^{-\frac{|x-3|}{0.2}} \quad (\text{A.3})$$

830 At the first time step $t = 1$, the strain energy is changing to

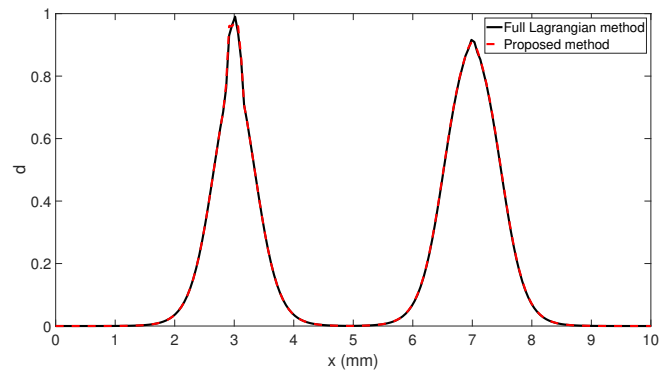
$$\psi_e^+(x, t = 1) = 5e^{-\frac{|x-3|}{0.05}} + e^{-\frac{|x-7|}{0.2}} \quad (\text{A.4})$$

831 This energy intends to create a thinner crack at $x = 3$ mm with a
 832 higher peak value and initiate a new crack at $x = 7$ mm. Hence,
 833 the damage field around the initial crack is decreased if the irre-
 834 versibility condition is not imposed. We use the proposed method
 835 to compute the corresponding damage fields. Figure A.19 depicts
 836 the crack profiles of different time steps. We can see that the dam-
 837 age field did not decrease with the proposed irreversibility imple-
 838 mentation. Compared to the full Lagrangian method, the damage
 839 field is indeed degraded with the proposed method, as shown in
 840 Figure A.19(b). Fortunately, the difference is limited by refining
 841 the mesh (Figure A.19(c)). The final mesh size is reasonable, as it
 842 is only slightly inferior to the internal crack length.

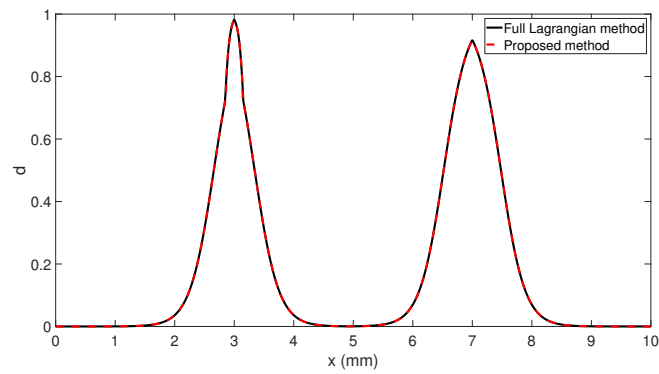
843



(a) $t = 0$, mesh size=0.05 mm



(b) $t = 1$, mesh size=0.05 mm



(c) $t = 1$, mesh size=0.01 mm

Figure A.19: Crack evolution in two meshes with comparison to full Lagrangian method

- 844 [1] A. A. Griffith, Vi. the phenomena of rupture and flow in solids, Philo-
845 sophical transactions of the royal society of london. Series A, containing
846 papers of a mathematical or physical character 221 (1921) 163–198.
- 847 [2] F. Yang, A. Rassineux, C. Labergere, K. Saanouni, A 3d h-adaptive
848 local remeshing technique for simulating the initiation and propagation
849 of cracks in ductile materials, *Computer Methods in Applied Mechanics
850 and Engineering* 330 (2018) 102–122.
- 851 [3] G. Gibert, B. Prabel, A. Gravouil, C. Jacquemoud, A 3d automatic
852 mesh refinement x-fem approach for fatigue crack propagation, *Finite
853 Elements in Analysis and Design* 157 (2019) 21 – 37.
- 854 [4] M. Elices, G. Guinea, J. Gomez, J. Planas, The cohesive zone model:
855 advantages, limitations and challenges, *Engineering fracture mechanics*
856 69 (2002) 137–163.
- 857 [5] N. Blal, L. Daridon, Y. Monerie, S. Pagano, Artificial compliance in-
858 herent to the intrinsic cohesive zone models: criteria and application to
859 planar meshes, *International journal of fracture* 178 (2012) 71–83.
- 860 [6] I. Babuška, J. M. Melenk, The partition of unity method, *International
861 journal for numerical methods in engineering* 40 (1997) 727–758.
- 862 [7] N. Moës, J. Dolbow, T. Belytschko, A finite element method for crack
863 growth without remeshing, *International journal for numerical methods
864 in engineering* 46 (1999) 131–150.
- 865 [8] N. Moës, A. Gravouil, T. Belytschko, Non-planar 3d crack growth by
866 the extended finite element and level sets—part i: Mechanical model,
867 *International journal for numerical methods in engineering* 53 (2002)
868 2549–2568.
- 869 [9] A. Gravouil, N. Moës, T. Belytschko, Non-planar 3d crack growth by
870 the extended finite element and level sets—part ii: Level set update,
871 *International journal for numerical methods in engineering* 53 (2002)
872 2569–2586.
- 873 [10] C. Miehe, M. Hofacker, F. Welschinger, A phase field model for rate-
874 independent crack propagation: Robust algorithmic implementation

- 875 based on operator splits, *Computer Methods in Applied Mechanics and*
876 *Engineering* 199 (2010) 2765–2778.
- 877 [11] G. A. Francfort, J.-J. Marigo, Revisiting brittle fracture as an energy
878 minimization problem, *Journal of the Mechanics and Physics of Solids*
879 46 (1998) 1319–1342.
- 880 [12] B. Bourdin, G. A. Francfort, J.-J. Marigo, Numerical experiments in
881 revisited brittle fracture, *Journal of the Mechanics and Physics of Solids*
882 48 (2000) 797–826.
- 883 [13] D. Mumford, J. Shah, Optimal approximations by piecewise smooth
884 functions and associated variational problems, *Communications on pure*
885 *and applied mathematics* 42 (1989) 577–685.
- 886 [14] L. Ambrosio, V. M. Tortorelli, Approximation of functional depending
887 on jumps by elliptic functional via t -convergence, *Communications on*
888 *Pure and Applied Mathematics* 43 (1990) 999–1036.
- 889 [15] C. Miehe, F. Welschinger, M. Hofacker, Thermodynamically consistent
890 phase-field models of fracture: variational principles and multi-field fe
891 implementations, *International Journal for Numerical Methods in En-*
892 *gineering* 83 (2010) 1273–1311.
- 893 [16] T.-T. Nguyen, J. Yvonnet, Q.-Z. Zhu, M. Bornert, C. Chateau, A
894 phase-field method for computational modeling of interfacial damage
895 interacting with crack propagation in realistic microstructures obtained
896 by microtomography, *Computer Methods in Applied Mechanics and*
897 *Engineering* 312 (2016) 567–595.
- 898 [17] L. Xia, D. Da, J. Yvonnet, Topology optimization for maximizing the
899 fracture resistance of quasi-brittle composites, *Computer Methods in*
900 *Applied Mechanics and Engineering* 332 (2018) 234–254.
- 901 [18] M. J. Borden, T. J. Hughes, C. M. Landis, C. V. Verhoosel, A higher-
902 order phase-field model for brittle fracture: Formulation and analysis
903 within the isogeometric analysis framework, *Computer Methods in Ap-*
904 *plied Mechanics and Engineering* 273 (2014) 100–118.

- 905 [19] V. Ziaei-Rad, Y. Shen, Massive parallelization of the phase field formu-
906 lation for crack propagation with time adaptivity, *Computer Methods*
907 *in Applied Mechanics and Engineering* 312 (2016) 224–253.
- 908 [20] S. Yulong, D. Qinglin, Q. Shasha, Adaptive consistent element-free
909 galerkin method for phase-field model of brittle fracture, *Computational*
910 *Mechanics* <https://doi.org/10.1007/s00466-019-01679-2> (2019).
- 911 [21] S. Burke, C. Ortner, E. Süli, An adaptive finite element approximation
912 of a variational model of brittle fracture, *SIAM Journal on Numerical*
913 *Analysis* 48 (2010) 980–1012.
- 914 [22] T. Heister, M. F. Wheeler, T. Wick, A primal-dual active set method
915 and predictor-corrector mesh adaptivity for computing fracture prop-
916 agation using a phase-field approach, *Computer Methods in Applied*
917 *Mechanics and Engineering* 290 (2015) 466–495.
- 918 [23] Y. Li, W. Lai, Y. Shen, Variational h-adaption method for the phase
919 field approach to fracture, *International Journal of Fracture* 217 (2019)
920 83–103.
- 921 [24] R. Patil, B. Mishra, I. Singh, An adaptive multiscale phase field method
922 for brittle fracture, *Computer Methods in Applied Mechanics and En-*
923 *gineering* 329 (2018) 254–288.
- 924 [25] F. Zhang, W. Huang, X. Li, S. Zhang, Moving mesh finite element
925 simulation for phase-field modeling of brittle fracture and convergence
926 of newton’s iteration, *Journal of Computational Physics* 356 (2018)
927 127–149.
- 928 [26] T. Wick, Modified newton methods for solving fully monolithic phase-
929 field quasi-static brittle fracture propagation, *Computer Methods in*
930 *Applied Mechanics and Engineering* 325 (2017) 577–611.
- 931 [27] G. Molnár, A. Gravouil, 2d and 3d abaqus implementation of a ro-
932 bust staggered phase-field solution for modeling brittle fracture, *Finite*
933 *Elements in Analysis and Design* 130 (2017) 27–38.
- 934 [28] H. Amor, J.-J. Marigo, C. Maurini, Regularized formulation of the vari-
935 ational brittle fracture with unilateral contact: Numerical experiments,
936 *Journal of the Mechanics and Physics of Solids* 57 (2009) 1209–1229.

- 937 [29] M. Ambati, T. Gerasimov, L. De Lorenzis, Phase-field modeling of
938 ductile fracture, *Computational Mechanics* 55 (2015) 1017–1040.
- 939 [30] T. Helfer, B. Bary, T. T. Dang, O. Fandeur, B. Michel, Modélisation
940 par champ de phase de la fissuration des matériaux fragiles: Aspects
941 numériques et applications au combustible nucléaire oxyde, 13ème col-
942 loque national en calcul des structures (2017).
- 943 [31] P. Farrell, C. Maurini, Linear and nonlinear solvers for variational phase-
944 field models of brittle fracture, *International Journal for Numerical*
945 *Methods in Engineering* 109 (2017) 648–667.
- 946 [32] T. Gerasimov, L. De Lorenzis, On penalization in variational phase-field
947 models of brittle fracture, arXiv preprint arXiv:1811.05334 (2018).
- 948 [33] M. Wheeler, T. Wick, W. Wollner, An augmented-lagrangian method for
949 the phase-field approach for pressurized fractures, *Computer Methods*
950 *in Applied Mechanics and Engineering* 271 (2014) 69–85.
- 951 [34] G. Lancioni, G. Royer-Carfagni, The variational approach to fracture
952 mechanics. a practical application to the french panthéon in paris, *Jour-*
953 *nal of elasticity* 95 (2009) 1–30.
- 954 [35] B. Bourdin, C. J. Larsen, C. L. Richardson, A time-discrete model for
955 dynamic fracture based on crack regularization, *International journal of*
956 *fracture* 168 (2011) 133–143.
- 957 [36] C. J. Larsen, C. Ortner, E. Süli, Existence of solutions to a regular-
958 ized model of dynamic fracture, *Mathematical Models and Methods in*
959 *Applied Sciences* 20 (2010) 1021–1048.
- 960 [37] M. J. Borden, C. V. Verhoosel, M. A. Scott, T. J. Hughes, C. M. Landis,
961 A phase-field description of dynamic brittle fracture, *Computer Methods*
962 *in Applied Mechanics and Engineering* 217 (2012) 77–95.
- 963 [38] W. Ye, A. Bel-Brunon, S. Catheline, M. Rochette, A. Combescure, A
964 selective mass scaling method for shear wave propagation analyses in
965 nearly incompressible materials, *International Journal for Numerical*
966 *Methods in Engineering* 109 (2017) 155–173.

- 967 [39] I. Ramière, T. Helfer, Iterative residual-based vector methods to acceler-
968 ate fixed point iterations, *Computers & Mathematics with Applications*
969 70 (2015) 2210–2226.
- 970 [40] B. Michel, T. Helfer, I. Ramière, C. Esnoul, A new numerical methodol-
971 ogy for simulation of unstable crack growth in time independent brittle
972 materials, *Engineering Fracture Mechanics* 188 (2018) 126–150.
- 973 [41] T. Helfer, B. Michel, J.-M. Proix, M. Salvo, J. Sercombe, M. Casella,
974 Introducing the open-source mfront code generator: Application to me-
975 chanical behaviours and material knowledge management within the
976 pleiades fuel element modelling platform, *Computers & Mathematics*
977 *with Applications* 70 (2015) 994–1023.
- 978 [42] S. Melin, Why do cracks avoid each other?, *International Journal of*
979 *Fracture* 23 (1983) 37–45.
- 980 [43] M.-É. Schwaab, T. Biben, S. Santucci, A. Gravouil, L. Vanel, Interacting
981 cracks obey a multiscale attractive to repulsive transition, *Physical*
982 *review letters* 120 (2018) 255501.
- 983 [44] P. Sicsic, J.-J. Marigo, C. Maurini, Initiation of a periodic array of cracks
984 in the thermal shock problem: a gradient damage modeling, *Journal of*
985 *the Mechanics and Physics of Solids* 63 (2014) 256–284.
- 986 [45] C. Jiang, X. Wu, J. Li, F. Song, Y. Shao, X. Xu, P. Yan, A study of the
987 mechanism of formation and numerical simulations of crack patterns in
988 ceramics subjected to thermal shock, *Acta Materialia* 60 (2012) 4540–
989 4550.